Title
Light-Activated Mesoporous Silica Nanoparticles for Nanoimpeller-Controlled and Photodynamic Cancer Therapy

Author
CHOI, EUNSHIL

Publication Date
2014

Peer reviewed|Thesis/dissertation

UNIVERSITY OF CALIFORNIA

Los Angeles

Light-Activated Mesoporous Silica Nanoparticles for Nanoimpeller-Controlled and Photodynamic Cancer Therapy

A dissertation submitted in partial satisfaction of the

requirements for the degree Doctor of Philosophy

in Chemistry

by

Eunshil Choi

2014

ABSTRACT OF THE DISSERTATION

Light-Activated Mesoporous Silica Nanoparticles for
Nanoimpeller-Controlled and Photodynamic Cancer Therapy

by

Eunshil Choi

Doctor of Philosophy in Chemistry

University of California, Los Angeles, 2014

Professor Jeffrey I. Zink, Chair

In the recent biomedical research, mesoporous silica nanoparticles (MSNs) prepared by sol-gel chemistry have useful applications in cancer treatment. This is because of several attractive aspects of the MSN such as uniform pores with tunable size, large surface area, ease in functionalization, and biocompatibility. Also when the pores are functionalized with organic molecules that are stimuli-responsive, a controlled release system can be obtained for storage and delivery of a wide range of drugs through the pores. Among many therapeutic MSNs, light-activated silica nanoparticles are advantageous because ease in applying light activation allows for control of the system at a distance and a desired time. MSNs discussed in this dissertation involve two different types of the photo-responsive behaviors of functional molecules: (1)

controlled release of pore contents by azobenzene-based nanoimpellers, and (2) generation of reactive oxygen species (ROS) by porphyrin-based photosensitizers.

Nanoimpeller-controlled MSNs, which are a main focus of this dissertation, are discussed in Chapter 2-4. Nanoimpellers consist of photo-responsive azobenzene derivatives that are attached to the mesopores, and undergo photoiosmerization that results in dynamic wagging motions of the unbound termini and drives the expulsion of molecules from the pores. Controlled release of molecules is demonstrated in solution using fluorescent dyes (Chapter 2) and then in human cancer cells using an anticancer drug to induce cell death (Chapter 3). Various molecules having different water solubilities are tested in non-aqueous, aqueous, and intracellular environments as well (Chapter 4). The last part of the dissertation illustrates photosensitizer-functionalized MSNs for photodynamic therapy (PDT). A photosensitizer porphyrin derivative that is bonded to the pore wall is operated to generate singlet oxygen by light irradiation to treat malignant cells (Chapter 5).

The dissertation of Eunshil Choi is approved.

Richard Kaner

Michael A. Jura

Jeffrey I. Zink, Committee Chair

University of California, Los Angeles

2014

TABLE OF CONTENTS

ACKNOWLEDGEMENTS

Despite my strong aptitude for science, it has not been an easy journey to pursue a Ph. D. degree in chemistry. Life as a graduate student has been much more than studying assigned textbooks, similar to college. It has required a lot of patience and courage to go through numerous trials and errors in research.

Finally as I am here to write up my dissertation and look back upon my past years at UCLA, I would first like to give my sincere gratitude to my research advisor, Dr. Jeffrey I. Zink. He has not only offered his best support on my research, but has also been a very generous counselor when I encountered personal hardships. Thank you so much for not giving up on me during difficult times. I learned a priceless lesson from you about having the attitude to become a good chemist for life.

I would like to thank my committee members Dr. Richard Kaner, Dr. Michael Jura, and Dr. Ohyun Kwon too. Thank you so much for your time in attending my oral examination and reading this dissertation.

I would also like to convey my gratitude to my research co-workers, Dr. Fuyuhiko Tamanoi and Dr. Jie Lu for biomedical research. Thank you so much for being willing to offer your hands whenever I brought up with a new synthesized nanoparticle. Without your dedications in cell studies, my research could not be complete. I also thank my current colleagues in the Zink laboratory, Janie Chen, Juyao Dong, Tania Guardado, Angela Hwang, Matt Kiesz, Zilu Li, Phillippe Saint-Cricq-Riviere, and Chia-Jung Yu (names listed in the alphabetical order). It was great having all of you as my colleagues during my time at UCLA.

Beside people in the scientific community, I would like to acknowledge those who I have met outside of campus, especially at church. To pastor Soon and Esther, thank you so much for your continuous care for me and my spiritual strength. Thanks to you, I have reset my mind to find a real joy in life. To Korean cell members, thank you for always being there as a solid community. To the running club members, especially Coach Akio Yamada, thank you so much for helping me to stay physically strong through marathon training. To all church members, thank you for influencing me with your mature Christianity.

To my parents. Thank you so much for your unconditional love to me, and continuous support on my dream. You are the strongest motivation for my life.

My last acknowledgment goes to my Lord and Savior Jesus Christ. Without your guidance, this dissertation would not have been possible.

VITA

2003	B.S. Chemistry (*Summa cum Laude*) Inha University Incheon, Republic of Korea
2005	M.S. Physical Chemistry Korea Advanced Institute of Science and Technology (KAIST) Daejeon, Republic of Korea
2006-2010, 2012-2014	Ph. D. program, Inorganic Chemistry Research/Teaching Assistant Department of Chemistry and Biochemistry University of California Los Angeles (UCLA) Los Angeles, USA

PUBLICATIONS

(* Co-First author)

[1] **Choi, E**.; Lu, J.; Tamanoi, F.; Zink, J. I.; Drug Release from Three-Dimensional Cubic Mesoporous Silica Nanoparticles Controlled by Nanoimpellers, Zeitschrift für Anorganische und Allgemeine Chemie, 2014, online published

[2] Liong, M.; Angelos, S.; **Choi, E**.; Kaushik, P.; Stoddart, J. F.; Zink, J. I.; Mesostructured multifunctional nanoparticles for imaging and drug delivery**,** *J. Mater. Chem*.**,** 2009, *19*, 6251

[3] Klichko, Y.; Liong, M.; **Choi, E.**; Angelos, S.; Nel, A. E.; Stoddart, J. F.; Tamanoi, F.; Zink, J. I.;Mesostructured Silica for Optical Functionality, Nanomachines, and Drug Delivery; *J. Am. Ceram. Soc*., 2009, *92*, S2

[4] Lu, J.; **Choi, E.***; Tamanoi, F.; Zink, J. I.; Light-Activated Nanoimpeller-Controlled Drug Release in Cancer Cells, *Small*, 2008, *4*, 421

[5] Johansson, E.; **Choi, E**.; Angelos, S.; Liong, M.; Zink, J. I.; Light-Activated Functional Mesostructured Silica, *J. Sol-Gel Sci Tech*, 2008, *46*, 313

[6] Angelos, S.; Liong, M.; **Choi, E**.; Zink, J. I.; Mesoporous Silicate Materials as Substrates for Molecular Machines and Drug Delivery; *Chem. Eng. J.,* 2008, 137, 4

[7] Angelos, S.; **Choi, E.**; Voegtle, F.; De Cola, L.; Zink, J. I.; Photo-Driven Expulsion of Molecules from Mesoporous Silica Nanoparticles; *J. Phys. Chem. C*, 2007, *111*, 6589

PATENT

[1] Zink, J. I.; Tamanoi, F.; **Choi, E.**; Angelos, S.; Kabehie, S.; Nel, A.; Lu, J.; Nano-Devices Having Impellers for Capture and Release of Molecules; WO/2009/094568

CHAPTER 1.

Introduction

1.1. Mesoporous Silica Nanoparticles (MSNs) for Biomedical Applications

In the field of biomedicine, mesoporous silica nanoparticles (MSNs) synthesized by sol-gel methodology[1–3] have gained a great deal of attention from researchers because of the several advantageous characteristics. Above all, the uniform mesopores with tunable sizes (c.a. 1 – 10 nm) and large surface area (up to more than 1000 m^2g^{-1}) allow for the storage of cargo molecules in a high loading capacity.[4] Also, surface compositions of the silica framework can be varied with a wide range of organic molecules along the pore walls or on the exposed particle surfaces.[5] The surface modification does not only allow for diverse cargo loading, but also offers the opportunity of creating a variety of bio-functionalities.[6] Furthermore, MSNs have low degradability with high chemical and thermal stabilities, making it possible to produce the particles in a large scale, and to store for a long period of time and then use them in need. Examples of biomedical applications of the MSNs include cell markers, and delivery of therapeutic agents and biomolecules (e.g. genes and proteins).[7–14]

In order to maximize cellular uptake and biofunctional efficiency of the MSN, it is crucial to obtain desirable morphologies such as monodisperse spherical shapes and smaller sizes of the particles.[15] When mesoporous silica was first reported in the early 1990s by the Mobil researchers, it was in a hexagonal prism shape with a large size (~2 μm).[1] After that, synthesis of the submicrometer sphere of mesoporous silica was first reported by Grun et al. in the later 1990s.[16] The particles, however, were in the agglomerated form, which has a poor solubility in aqueous media. With rapid progress in the MSN-based biological research in the last decade, the MSNs of ~ 100 nm or less in diameter have recently become available by several synthetic techniques (e.g. use of co-surfactant and polymer coating, and control of reactant ratio) and

tested in a variety of *in vitro* and *in vivo* cell studies.[15,17–20]

1.1.1. Synthesis and Characterization of MSN

Mesoporous silica materials can be easily synthesized by a base-catalyzed sol-gel method[21] that involves two steps of reactions, hydrolysis and condensation of alkoxysilane (silica precursor) in aqueous solution:

(1) Hydrolysis: $Si(OR)_4 + 4H_2O \rightarrow Si(OH)_4 + 4ROH$

(2) Condensation: $nSi(OH)_4 \rightarrow nSiO_2 + 2nH_2O$

Alkoxysilane $Si(OR)_4$ molecules are first hydrolyzed to silanolic acid $Si(OH)_4$ with water. Hydrolized alkoxysilanes then undergo condensation polymerization to form Si-O-Si bonds in the infinite network. When a pore-templating surfactant is added to the process before the hydrolysis step, condensation of the alkoxysilane molecules occurs around the self-assembled micelles of the surfactant molecules, which results in the formation of porous silica. The size and structure of the pores can be varied with adjustment of synthetic conditions (e.g. temperature, surfactant, and solvent).[22,23] The as-synthesized materials are then refluxed in acidic alcohol to remove the surfactant and obtain the empty mesopores (Figure 1.1).

Physical properties of the synthesized particles are characterized by a series of equipment measurement, as summarized below.

(1) X-ray diffraction: d-spacing and structure of the pores
(2) Scanning (Transmission) electronic microscopy: shapes and sizes of the particles

(3) Fourier Transform-Infrared spectroscopy: surfactant-free pores

(4) Dynamic light scattering: dispersity and average size of the particles

(5) Gas sorption: surface area of the particles, size and volume of the pores, and formation of the porosity

1.1.2. MCM-41 vs. MCM-48

A typically synthesized form of the MSN has a well-ordered structure of tubular pores in the two-dimensional *p6mm* hexagonal phase. The silica with this form of the pores is called MCM-41, which was named after the researchers' affiliations in 1992.[1] When the acronym MSN is used in this thesis, it usually indicates the MCM-41. On the other hand, another form of the mesopores consists of enatiomeric pairs of tubular pores that are continuously interwoven and branched to each other, forming a three-dimensional *Ia3d* cubic phase of the pores. The mesoporous silica with the cubic pores is called MCM-48. Either pore phase can be favorably synthesized depending on the condition of the surfactant during the sol-gel process, represented by the packing parameter g as a function of the total volume and the tail length of the hydrophobic region, and the hydrophilic head group area of the self-assembled surfactant micelle. In comparison, a higher g value results in the cubic mesostructure of the particles.[24]

1.1.3. Functionalization of the MSN

The MSNs can be functionalized with various organic molecules, which contain alkoxylsilane groups that are capable of forming a chemical bond to the silica framework.[25] Depending on whether the molecules are placed inside the pores or on the external surfaces of the particles, a synthetic strategy can be chosen between the co-condensation and the post-

synthetic grafting method.[26]

1.1.3.1. Co-condensation Strategy

This strategy is used to functionalize the interiors of the mesopores. The method takes advantages of bifunctionality[5] of the surfactant during the sol-gel process. It is a well-known phenomenon that the surfactant molecules are self-assembled in water with the hydrophobic tails aggregated toward the center and the ionic heads remaining in contact with water.[1] When alkoxysilane molecules containing organic functional moieties are added to this surfactant solution, the hydrophobic organic moieties are placed to interact with the water-insoluble surfactant chains, and hydrophilic silanol groups are exposed to undergo condensation with water.[25] In a well-established method in the Zink laboratory,[26] organosilanes are added to the surfactant solution together with a silica precursor tetraethylorthosilicate (TEOS) such that both silanes are allowed to co-condense into the silica framework. After the surfactant is removed, the empty pores are obtained with the organic molecules attached to the pore walls.

1.1.3.2. Post-synthetic Grafting Method

This technique is employed for functionalization of the external surfaces of the particles. Unlike the co-condensation approach, this method involves two steps of the procedure: synthesis of unfunctionalized surfactant-free particles, and treatment of the particles with functional molecules. This method is useful for attachment of functional molecules in a larger dimension to the MSN. For example, supramolecular nanovalve systems[27–29] are installed on the pore entrances on the exposed silica surfaces by this strategy. Examples of the molecules also include

biologically useful molecules such as fluorescent molecules (e.g. Rhodamine B or Fluorescein-derivatized organosilane) for intracellular imaging of the particles.[30]

1.2. Light-Activated MSNs for Cancer Therapy

Among various biomedical applications of the MSNs, cancer treatment has been a key issue area that still requires a lot of investigations. Because most of the therapeutic agents are hydrophobic and poorly dissolved in biological media (i.e. at neutral pH), they have been limited for clinical applications. Recently developed biocompatible MSN-based drug delivery systems have been able to load those drugs in the mesopores and successfully deliver them into cancer cells to induce cell apoptosis without damaging healthy cells.[6,18,31] Especially when the MSNs were associated with active molecules that are able to respond to certain stimuli (e.g. pH[29,32–35], light[26,31,36–41], magnetism[42,43], and so forth[27,28,44]), mechanized drug delivery systems (i.e. molecular machine) could be constructed, enabling sophisticated control of the drug release from the particles. Among the diverse sources of the stimuli, light is advantageous compared to others because it can be switched on and off easily and promptly on demand, which makes the system controllable at a distance and at a desired time. The light-activated MSNs discussed in this dissertation are based on two different types of the response behavior of the functional molecules to the light stimuli: (1) a large amplitude motion for controlled release of the pore contents operated by the nanoimpeller mechanism[26], and (2) a generation of reactive oxygen species (ROS) for the photodynamic therapy (PDT).[45]

1.2.1. Nanoimpeller-based Drug Delivery

The first type of the materials, which is a main focus of this dissertation, is based on the nanoimpeller mechanism[26,30,31] that involves a large amplitude dynamic motion of the photo-excited functional group. Nanoimpeller was first invented in 2007 by the author under supervision of Professor Jeffrey I. Zink, to realize the mechanized system that is able to control the trap and release of molecules on external command.[26] The nanoimpeller-functionalized MSN consists of photo-responsive azobenzene derivatives that are attached to the silica framework.

Azobenzene is composed of two benzene rings connected by the covalent N=N bond. Since the cis-conformer of azobenzene was first discovered in 1937 by Hartley,[46] it has been well known that the two conformers of azobenzene (i.e. trans and cis isomer) exhibit reversible photoisomerization around the N=N bond at specific wavelengths of a light. In an earlier work in the Zink research group, photochemistry of azobenzenes attached to mesoporous silica was studied in detail, and their absorption spectra were obtained.[47] Two characteristic peaks of the azobenzene in the visible and UV regions are assigned to the two electronic transitions: a strong π-π* transition around 350 nm (leading to trans to cis isomerization) and a weak n-π* transition around 450 nm (leading to cis to trans conversion) (Figure 1.3).

In Chapters 2-4, nanoimpellers on synthesis, characterization, and controlled release experiments are discussed. In an effort to optimize the system for intracellular investigations, different particle morphologies are have been studied with different sizes and structures of the pores. First of all, Chapter 2 illustrates the first design of the nanoimpeller to realize photo-driven expulsion of molecules, which is built on the MSN having ~ 2nm mesopores in the two-

dimensional hexagonal phase. In comparison to the impeller, another azobenzene-functionalized MSN that is operated by a different mechanism (i.e. gatekeeper mechanism) is exhibited as well. Using both systems, controlled release of laser dyes from the mesopore into solution is monitored by fluorescence spectroscopy. This chapter is a revised version of the manuscript published in *Journal of Physical Chemistry C*, written by Sarah Angelos, Eunshil Choi, Jeffrey I. Zink, et al., which the author contributed to by synthesizing the nanoimpeller.[26]

In Chapter 3, the nanoimpeller is utilized to deliver an anticancer drug camptothecin (CPT) into living cells to induce cell apoptosis. For this study, the MSN was synthesized with a smaller size of the hexagonal pores (c.a. 1.8 nm) to minimize the leakage of the drug and maximize the drug release efficiency in various human cancer cells. This chapter is a revised version of the manuscript published in *Small*, written by Jie Lu*, Eunshil Choi*, Fuyuhiko Tamanoi and Jeffrey I. Zink (* co-first author).[31]

Lastly Chapter 4 shows drug release from a different type of the mesostructure (i.e. three-dimensional *Ia3d* cubic pore phase of the MSN[22]) functionalized with both nanoimpeller and a fluorescent molecule Rhodamine B-isothiocyanate (RITC). It is demonstrated that diverse cargo molecules having different hydrophilicities are controllably released from the particles in aqueous, non-aqueous, and intracellular environment. This chapter is a re-formatted version of the manuscript published in *Zeitschrift für Anorganische und Allgemeine Chemie,* written by Eunshil Choi, Jie Lu, Fuyuhiko Tamanoi, and Jeffrey I. Zink.[30]

1.2.2. Photodynamic Therapy (PDT)

Unlike the nanoimpeller that is designed to trap and release drug molecules, the PDT system contains a photosensitizing agent that is able to produce reactive oxygen species (ROS) to treat malignant cells. The MSNs discussed in Chapter 5 are functionalized with a photosensitizer porphyrin derivative along the pore walls. It is demonstrated that a synergetic cancer treatment can be achieved when this MSN is loaded with an anticancer drug CPT and exposed to the light to excite porphyrin. This is an unpublished work accomplished by the author.

1.3. Figures

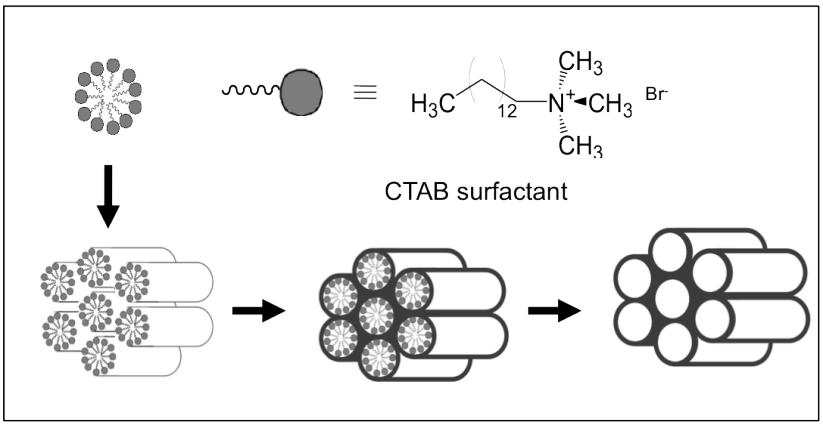

Figure 1.1. Sol-gel process to synthesize MSNs with a hexagonal array of tubular pores. The cationic surfactant cetyltrimethylammonium bromide (CTAB) is self-assembled in aqueous solution to form a two-dimensional hexagonal phase of the tubular pores. Then a silica precursor alkoxysilane is added to the surfactant solution for condensation polymerization around the micelles. After the surfactant removal, the MSN is obtained with empty pores.

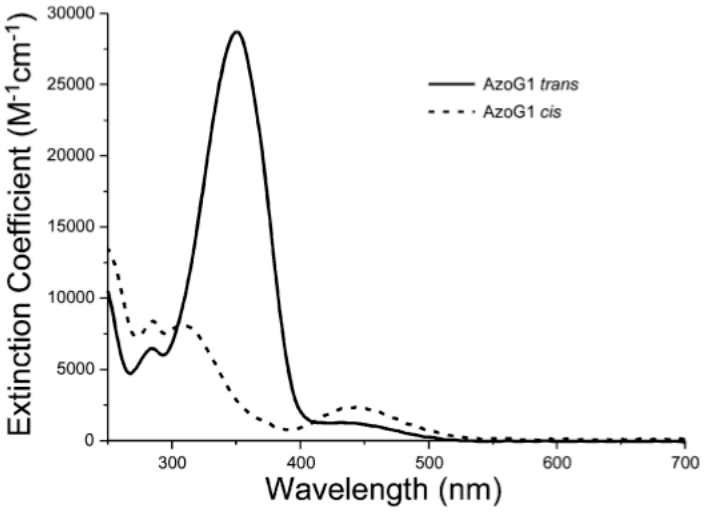

Figure 1.2. Extinction spectra of the trans and cis isomers of AzoG1 attached to mesoporous silica. AzoG1 means azobenzene derivatized with generation one of the Fre´chet Dendron. Two peaks appeared in the UV-Vis regions correspond to trans to cis isomerization (around 350 nm) and cis to trans conversion (around 450 nm).

1.4. References

[1] J. S. B. C.T. Kresge, M.E. Leonowicz, W.J. Roth, J.C. Vartuli, *Nature* **1992**, *359*, 710–712.

[2] M. H. Huang, B. S. Dunn, H. Soyez, J. I. Zink, **1998**, 7331–7333.

[3] Y. Lu, R. Ganguli, C. Drewien, M. Anderson, J. I. Zink, *Nature* **1997**, *389*, 651–655.

[4] Z. Li, J. N. Likoko, A. a Hwang, D. P. Ferris, S. Yang, G. Derrien, C. Charnay, J.-O. Durand, J. I. Zink, *J. Phys. Chem. C. Nanomater. Interfaces* **2011**, *115*, 19496–19506.

[5] S. Angelos, E. Johansson, J. F. Stoddart, J. I. Zink, *Adv. Funct. Mater.* **2007**, *17*, 2261–2271.

[6] M. Liong, S. Angelos, E. Choi, K. Patel, J. F. Stoddart, J. I. Zink, *J. Mater. Chem.* **2009**, *19*, 6251.

[7] C.-Y. Lai, B. G. Trewyn, D. M. Jeftinija, K. Jeftinija, S. Xu, S. Jeftinija, V. S.-Y. Lin, *J. Am. Chem. Soc.* **2003**, *125*, 4451–9.

[8] Y.-S. Lin, C.-P. Tsai, H.-Y. Huang, C.-T. Kuo, Y. Hung, D.-M. Huang, Y.-C. Chen, C.-Y. Mou, *Chem. Mater.* **2005**, *17*, 4570–4573.

[9] M. Arruebo, M. Gala, N. Navascue, C. Te, C. Marquina, M. R. Ibarra, **2006**, 1911–1919.

[10] K. Weh, J. Caro, M. Noack, K. Hoffmann, K. Schr, **2002**, *54*, 15–26.

[11] E. Besson, A. Mehdi, D. Lerner, C. Rey, R. J. P. Corriu, *J. Mater. Chem.* **2005**, *15*, 803.

[12] D. R. Radu, C.-Y. Lai, K. Jeftinija, E. W. Rowe, S. Jeftinija, V. S.-Y. Lin, *J. Am. Chem. Soc.* **2004**, *126*, 13216–7.

[13] I. I. Slowing, B. G. Trewyn, V. S.-Y. Lin, *J. Am. Chem. Soc.* **2007**, *129*, 8845–9.

[14] C. E. Ashley, E. C. Carnes, G. K. Phillips, D. Padilla, P. N. Durfee, P. A. Brown, T. N. Hanna, J. Liu, B. Phillips, M. B. Carter, et al., *Nature* **2011**, *10*, 389–397.

[15] H. Meng, M. Xue, T. Xia, Z. Ji, D. Y. Tarn, J. I. Zink, A. E. Nel, *ACS Nano* **2011**, *5*, 4131–44.

[16] M. Grun, I. Lauer, K. K. Unger, *Adv. Mater.* **1997**, *9*, 254–257.

[17] H. Meng, M. Xue, T. Xia, Y.-L. Zhao, F. Tamanoi, J. F. Stoddart, J. I. Zink, A. E. Nel, *J. Am. Chem. Soc.* **2010**, *132*, 12690–7.

[18] J. Lu, M. Liong, J. I. Zink, F. Tamanoi, *Small* **2007**, *3*, 1341–6.

[19] H. Meng, M. Liong, T. Xia, Z. Li, Z. Ji, J. I. Zink, A. E. Nel, *ACS Nano* **2010**, *4*, 4539–50.

[20] J.-K. Hsiao, C.-P. Tsai, T.-H. Chung, Y. Hung, M. Yao, H.-M. Liu, C.-Y. Mou, C.-S. Yang, Y.-C. Chen, D.-M. Huang, *Small* **2008**, *4*, 1445–52.

[21] L. L. Hench, J. K. West, *Chem. Rev.* **1990**, *90*, 33-72.

[22] B. K. Schumacher, F. Von Hohenesche, K. K. Unger, R. Ulrich, A. Du Chesne, U. Wiesner, H. W. Spiess, *Adv. Mater.* **1999**, *11*, 1194–1198.

[23] C. C. Landry, S. H. Tolbert, K. W. Gallis, A. Monnier, G. D. Stucky, P. Norby, J. C. H. O, N. York, **2001**, 1600–1608.

[24] Q. Huo, D. I. Margolese, G. D. Stucky, *Chem. Mater.* **1996**, *4756*, 1147–1160.

[25] S. Huh, J. W. Wiench, J. Yoo, M. Pruski, V. S. Lin, *Chem. Mater.* **2003**, *15*, 4247–4256.

[26] S. Angelos, E. Choi, F. Vo, L. De Cola, J. I. Zink, *J. Phys. Chem. C* **2007**, *111*, 6589–6592.

[27] K. C. Leung, T. D. Nguyen, J. F. Stoddart, J. I. Zink, *Chem. Mater.* **2006**, *18*, 5919–5928.

[28] T. D. Nguyen, H.-R. Tseng, P. C. Celestre, A. H. Flood, Y. Liu, J. F. Stoddart, J. I. Zink, *Proc. Natl. Acad. Sci. U. S. A.* **2005**, *102*, 10029–34.

[29] T. D. Nguyen, K. C.-F. Leung, M. Liong, C. D. Pentecost, J. F. Stoddart, J. I. Zink, *Org. Lett.* **2006**, *8*, 3363–6.

[30] E. Choi, J. Lu, F. Tamanoi, J. I. Zink, *Zeitschrift für Anorg. und Allg. Chemie* **2014**, online published.

[31] J. Lu, E. Choi, F. Tamanoi, J. I. Zink, *Small* **2008**, *4*, 421–426.

[32] D. Tarn, M. Xue, J. I. Zink, *Inorg. Chem.* **2013**, *52*, 2044–9.

[33] Y.-L. Zhao, Z. Li, S. Kabehie, Y. Y. Botros, J. F. Stoddart, J. I. Zink, *J. Am. Chem. Soc.* **2010**, *132*, 13016–25.

[34] N. M. Khashab, M. E. Belowich, A. Trabolsi, D. C. Friedman, C. Valente, Y. Lau, H. A. Khatib, J. I. Zink, J. F. Stoddart, *Chem. Commun. (Camb)*. **2009**, 5371–3.

[35] S. Angelos, N. M. Khashab, Y.-W. Yang, A. Trabolsi, H. A. Khatib, J. F. Stoddart, J. I. Zink, *J. Am. Chem. Soc*. **2009**, *131*, 12912–4.

[36] S. Angelos, Y.-W. Yang, N. M. Khashab, J. F. Stoddart, J. I. Zink, *J. Am. Chem. Soc*. **2009**, *131*, 11344–6.

[37] N. K. Mal, M. Fujiwara, Y. Tanaka, T. Taguchi, M. Matsukata, *Chem. Mater*. **2013**, *15*, 3385–3394.

[38] L. Mu, S. S. Feng, *J. Control. Release* **2003**, *86*, 33–48.

[39] S. Febvay, D. M. Marini, A. M. Belcher, D. E. Clapham, *Nano Lett*. **2010**, *10*, 2211–9.

[40] R. Huschka, O. Neumann, A. Barhoumi, N. J. Halas, *Nano Lett*. **2010**, *10*, 4117–22.

[41] D. P. Ferris, Y.-L. Zhao, N. M. Khashab, H. A. Khatib, J. F. Stoddart, J. I. Zink, *J. Am. Chem. Soc*. **2009**, *131*, 1686–8.

[42] C. R. Thomas, D. P. Ferris, J.-H. Lee, E. Choi, M. H. Cho, E. S. Kim, J. F. Stoddart, J.-S. Shin, J. Cheon, J. I. Zink, *J. Am. Chem. Soc*. **2010**, *132*, 10623–5.

[43] J. Kim, H. S. Kim, N. Lee, T. Kim, H. Kim, T. Yu, I. C. Song, W. K. Moon, T. Hyeon, *Angew. Chem. Int. Ed. Engl*. **2008**, *47*, 8438–41.

[44] J. Croissant, J. I. Zink, *J. Am. Chem. Soc*. **2012**, *134*, 7628–31.

[45] H.-L. Tu, Y.-S. Lin, H.-Y. Lin, Y. Hung, L.-W. Lo, Y.-F. Chen, C.-Y. Mou, *Adv. Mater*. **2009**, *21*, 172–177.

[46] G. S. Hartley, *Nature* **1937**, 281.

[47] P. Sierocki, H. Maas, P. Dragut, G. Richardt, F. Vögtle, L. De Cola, F. a M. Brouwer, J. I. Zink, *J. Phys. Chem. B* **2006**, *110*, 24390–8.

CHAPTER 2.

Photo-driven Expulsion of Molecules from

Mesoporous Silica Nanoparticles

2.1. Abstract

Azobenzene derivatives act as both impellers and gatekeepers when they are tethered in and on mesoporous silica nanoparticles. Continuous excitation at 457 nm, a wavelength where both the cis and trans conformers absorb, produces constant isomerization reactions and results in continual dynamic wagging of the untethered terminus. The 2 nm diameter pores are loaded with luminescent probe molecules, azobenzene motion is stimulated by light, and the photoinduced expulsion of the probe from the particles that is caused by the motion is monitored by luminescence spectroscopy. The light-responsive nature of these materials enables them to be externally controlled such that the expulsion of dye molecules from the mesopores can be started and stopped at will. These results open the possibilities of trapping useful molecules such as drugs and releasing them on demand.

2.2. Introduction

Control of molecular transport in, through, and out of mesopores has important potential applications in nanoscience including fluidics and drug delivery. Surfactant-templated silica[1] is a versatile material in which ordered arrays of mesopores can be easily synthesized, providing a convenient platform for attaching molecules that undergo large amplitude motions to control transport. Mesostructured silica is transparent (for photocontrol and spectroscopic monitoring), and can be fabricated into useful morphologies (thin films[2], particles[1,3]) with designed pore sizes and structures. One successful method of controlling transport uses the photo-induced cis-trans isomerization of N=N bonds in azobenzene derivatives tethered to the interiors of mesopores. To date, understanding of the light-responsive behavior of azobenzene-modified

materials has been based on a static mechanism, where the effective pore sizes are varied by azobenzene existing in the trans or cis conformation. In this chapter, it is shown that continuous excitation at 457 nm, a wavelength where both the cis and trans conformers absorb, produces constant isomerization reactions that cause continual dynamic wagging of the untethered terminus and impel molecules through the pores. In addition, it is shown that the dynamic control of transport can be made to occur in 400 nm diameter particles containing 2 nm diameter pores.

Mesostructured inorganic materials functionalized with azobenzene[4–9] have received significant attention owing to the photoactive responses of these hybrids, including control of the d-spacing of mesostructured materials.[5] Zeolitic membranes containing azobenzene were reported to exhibit photoswitchable gas permeation properties resulting from the trans-cis isomerization of azobenzene.[8] Mesostructured silicates synthesized with azobenzene-bridged pores exhibit light-responsive changes in adsorption ability correlating with the dimensional changes of azobenzene that occur upon photoisomerization.[9] Additionally, the transport rate of ferrocene derivatives through an azobenzene-modified cubic-structured silica film to an electrode was photoresponsively controlled by changing the effective pore size.[6]

A different type of transport control utilizes molecular machines with moving parts based on large amplitude molecular motions that are attached to the pore openings and act as gatekeepers. Gatekeepers based on supramolecular motifs where a cyclic component moves relative to a stationary thread,[10–13] on intermolecular dimerization of coumarin,[14,15] and on forming and breaking disulfide bonds[16] have been demonstrated. Sources of energy that have been used include pH changes,[10] redox chemical energy,[11] and competitive binding.[12]

In this chapter, it is demonstrated that the dynamic motion of azobenzene derivatives can be used to control the transport of molecules trapped in the mesopores of silica nanoparticles. The use of azobenzene derivatives is demonstrated as both impellers and gatekeepers in and on mesoporous silica nanoparticles, such that guest molecules are expelled from the particles under photocontrol. We designed spherical particles with diameters of about 400 nm, a small azobenzene derivative, AzoH (Figure 2.1), to attach to the pore interiors, and a larger azobenzene derivatized with a G1 Frechet dendron (AzoG1) to attach to the pore openings. Our prior photophysical studies have shown that switching of immobilized azobenzenes occurs inside of mesopores; the trans to cis isomerization quantum yield at 450 nm is 0.36 and that for cis to trans is 0.64.[17] Continuous excitation at this wavelength produces constant isomerization reactions and results in continual dynamic wagging of the untethered terminus. In the experiments reported here, azobenzene-modified pores are loaded with luminescent probe molecules, azobenzene motion is stimulated by light, and luminescence spectroscopy is used to monitor the photoinduced expulsion of the probe from the particles that is caused by the azobenzene motion. The relative efficiency of expulsion of the small probe molecules during radiation to retention in the dark is dependent on the position of the azobenzene in the pore, the concentration, and the size of the azobenzene moving part.

2.3. Results and Discussion

2.3.1. Synthesis and characterization of the azobenzene-derivatized MSNs

The solid supports for the azobenzene machines are ~ 400 nm diameter particles that contain ordered 2D hexagonal arrays of tubular pores (4 nm lattice spacing) prepared by a base catalyzed sol-gel method.[1,3] The pores are templated by cetyltrimethylammonium bromide (CTAB) surfactants, and tetraethylorthosilicate (TEOS) is used as the silica precursor. Empty pores are obtained by template removal using solvent extraction or calcination, and confirmed by FTIR spectroscopy (Figure 2.2). The ordered structure of the mesopores is confirmed by X-ray diffraction and the particle morphology by scanning electron microscopy (Figure 2.3).

Two synthetic approaches were chosen to derivatize the silica in the desired region. To evenly derivatize the interiors of the mesopores, azobenzene was first coupled to the linker molecule isocyanatopropyltriethoxysilane (ICPES), and the machine-linker species was then added to the sol during particle synthesis and allowed to cocondense into the silica framework. The template was removed by solvent extraction. This synthetic approach will be termed the co-condensation method (CCM). Formation of the chemical linkage between ICPES and azobenzene was confirmed by NMR spectroscopy (Figure 2.4), and attachment of the coupled ICPES-azobenzene to the silica was proven by UV-Vis spectroscopy (Figure 2.5). To attach the AzoG1 primarily at the pore openings, the calcined mesostructed particles were treated with ICPES followed by coupling. The large azobenzenes cannot penentrate deep inside the pores and the first to react block access to the rest. This approach will be termed the post-synthesis modification method (PSMM).

2.3.2. Photo-driven release of dyes from the azobenzene-functionalized MSNs

In order to use the azobenzene motion as an impeller, the small AzoH was attached onto the pore interiors using the CCM. Real time measurements of the rate of expulsion of two different dyes, Coumarin 540A (C540A) and Rhodamine 6G (R6G), were made. The pores were loaded with dye molecules by soaking the particles in 1 mM solutions of the dye overnight and then washed to remove adsorbed molecules from the surface. 15 mg of dye-loaded particles were placed in the bottom of a cuvette and 12 mL of MeOH was carefully added. A 1 mW, 457 nm probe beam directed into the liquid was used to excite dissolved dye molecules that are released from the particles (Figure 2.6). The spectrum was recorded as a function of time at 1 sec intervals. After 5 minutes, a 9 mW, 457 nm excitation beam was used to directly irradiate the functionalized particles and excite the azobenzenes' motion. Release of the dye was measured by the luminescence intensity of the dye dissolved into solution, at the emission maximum as functions of time (Figure 2.7). This release profile indicates that the particles hold the guest molecules but expel them when stimulated (Figure 2.8.a). As a control experiment to verify that azobenzene excitation drives the release, the particles were irradiated with equal power at a wavelength (647 nm) at which the azobenezene does not absorb. The red light had no effect on the release. These results demonstrate that the system only responds to wavelengths that drive the large amplitude azobenzene motion.

2.3.2.1. Impeller mechanism

The expulsion of molecules from pores containing azobenzene molecules attached internally probably involves an "impeller" mechanism. Prior to excitation, dye molecules are held inside the particles because the pores are considerably congested by the static azobenzene

machines and a facile pathway for escape is not available. Excitation of the azobenzenes causes them to wag back and forth, effectively imparting motion to the trapped dye molecules and allowing them to traverse the pore interior until they escape. The concentration at which azobenzene machines are tethered to the pore interiors determines the amount of congestion inside the mesopores, and therefore affects the ability to trap dye molecules in the dark. The effective concentration of the AzoH machines tethered inside the mesopores can be varied by changing the amount of the AzoH-ICPES precursor that is added to the TEOS sol during particle synthesis. When particles are prepared such that the concentration of azobenzene molecules doped into the pores is decreased by a factor of three, very slow diffusion of the dye molecules through the pores occurs in the dark and the system is leaky. It is likely that the decreased amount of azobenzene creates enough free space inside the mesopore such that the dye molecules can diffuse around in the dark, and are never completely trapped.

2.3.2.2. Gatekeeper mechanism

A second method of exploiting dynamic motion is to attach larger azobenzene derivatives at the pore orifices such that the machines can gate the pore openings in the dark. Static large molecules clog the entrances, but dynamic movement could provide intermittent openings for small molecules to slip through. In this gatekeeping approach, the size of the machine selected is a critical factor affecting nanovalve operation. The azobenzene derivative must be sufficiently large such that it can block the nanopore entrances when it is static, and mobile enough when irradiated to provide openings through which molecules can escape. AzoG1 was selected because its 1 nm size suggested that several would be sufficient to block the 2 nm pores.

Minimal leakage of probe molecules is observed prior to excitation but irradiation allows rapid escape (Figure 2.8.b). The smaller derivative AzoH does not sufficiently block the openings and leakage is observed when the molecules are static.

The fact that the dynamic motion responsible for controlling molecular transport can be photoresponsively turned on and off enables the systems to be externally regulated such that the expulsion of dye molecules from the mesopores can be started and stopped at will. The release profile of C540A from AzoG1-treated particles where the excitation is sequentially turned on and off is shown in Figure 2.8.c. The pore openings are adequately blocked in the dark and dyes are expelled from the particles only upon excitation of the AzoG1. The release experiments were repeated with a different dye R6G, which led to a similar pattern of the release profiles to that for C540A (Figure 2.9). Remote control of the flow of molecules out of mesopores is thus demonstrated.

2.4. Summary

The functional nanoparticles described here utilize the photo-controllable static and dynamic properties of azobenzene derivatives in and on mesopores. Luminescent probe molecules enable the function to be sensitively monitored. These results open up possibilities of trapping useful molecules such as drugs and releasing them on demand.

2.5. Experimental

For all the syntheses, reagents were purchased from Aldrich and used as received with the exception of PhMe and ICPES, which were purified by distillation. The synthesis of AzoG1 has been previously reported.[17]

2.5.1. Preparation of AzoH-modified materials via the CCM

The synthesis of AzoH-modified materials is derived from a previously reported synthetic methodology.[18] 4-phenylazoaniline was first reacted with ICPES to form a carbamide linkage by refluxing 0.2840 g of the azo with 1.42 mL of ICPES in 10mL of EtOH under N_2 for 4 h. During the coupling reaction, a surfactant solution[3] was prepared in the other flask: 2.0 g of CTAB, 7.0 mL of 2 M NaOH, and 480 g of the deionized H_2O were mixed and stirred for 30 min at 80 °C. To this solution, 9.34 g of the tetraethylorthosilicate (TEOS) and the coupled AzoH-ICPES machine were slowly added with vigorous stirring. After 2 h of stirring at 80 °C, the particles were filtered and thoroughly washed with MeOH and deionized H_2O. Template removal was accomplished by suspending 1 g of the as-synthesized particles in 100 mL of MeOH with 1 mL of concentrated HCl and heating at 60 °C for 6 h.

2.5.2. Preparation of AzoG1-modified materials via the PSMM

Pure mesoporous silica nanoparticles were prepared according to published literature procedure.[3] The CTAB surfactant was removed by calcination at 550 ˚C for 5 h. Attachment of the ICPES linker was accomplished by suspending 100 mg of the calcined particles in 10 mL of a 10 mM solution of ICPES in dry PhMe and refluxing for 12 h under N_2. ICPES-modified particles were filtered and thoroughly washed with PhMe and then placed in a 1 mM solution of

AzoG1 in PhMe and refluxed for 12 h under N_2. The AzoG1-modified particles were recovered by filtration, washed thoroughly with PhMe, and then dried under vacuum.

2.6. Figures

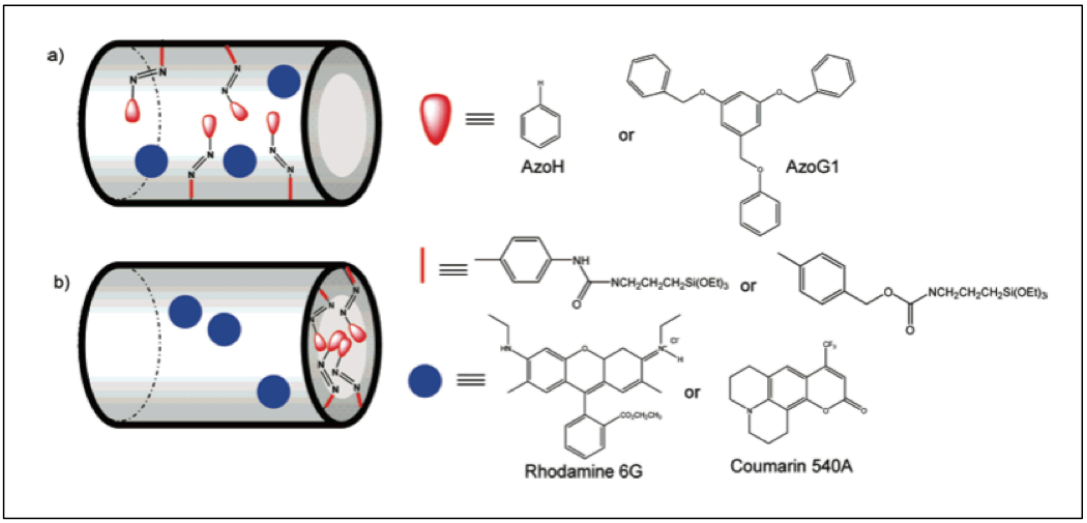

Figure 2.1. Photoresponsive materials functionalized with azobenzene derivatives. (a) Materials prepared by the CCM are derivatized with AzoH; (b) materials prepared by the PSMM are derivatized with AzoG1. For each system, the moveable phenyl ring of the azobenzene machine is illustrated by the red inverse teardrop, the tethered phenyl ring of the azobenzene machine by the red vertical bar, and the impelled molecule by the blue circle.

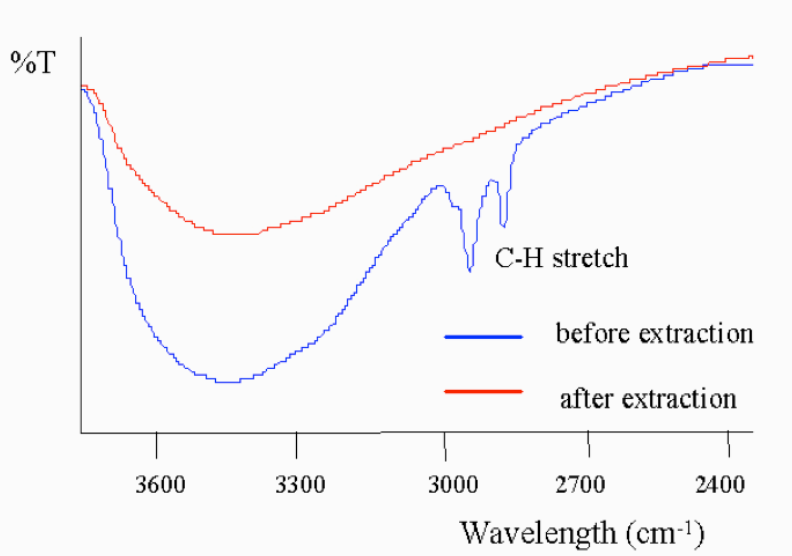

Figure 2.2. FT-IR spectrum of AzoH-modified particles before and after the solvent extraction. The two sharp peaks between 2,700 and 3,000 cm^{-1} are not present after the solvent extraction process, which indicates that the CTAB surfactant is completely removed and the empty mesopore is obtained.

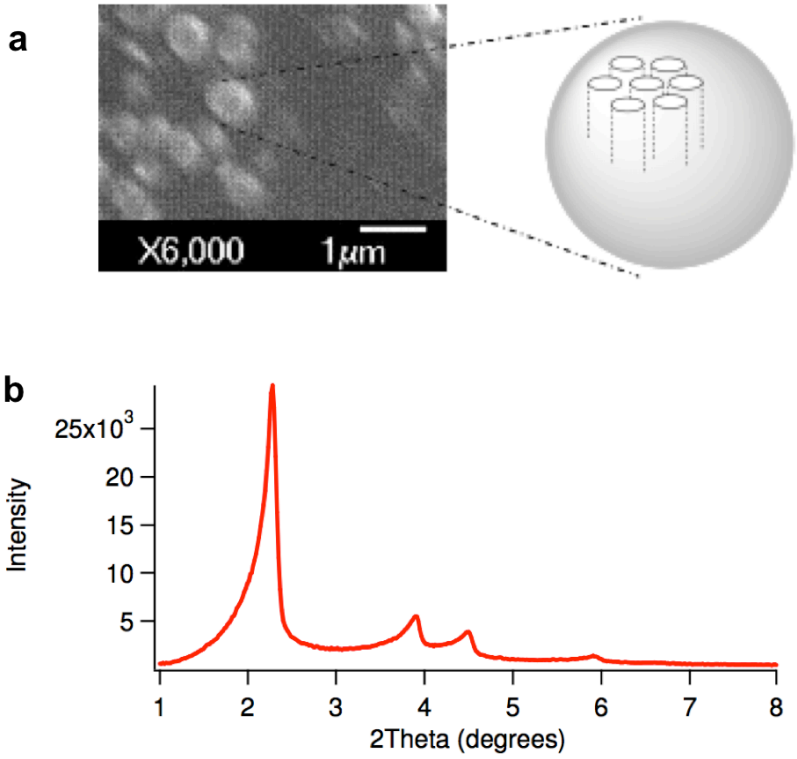

Figure 2.3. (a) SEM image of silica nanoparticles and illustration of the 2D hexagonal mesostructure. (The 2 nm diameter pores are not drawn to scale) (b) XRD pattern of AzoH-modified particles after solvent extraction. The 100 peak at $2\theta = 2.28^\circ$ corresponds to a 2D hexagonal structure with a lattice spacing of 3.9 nm.

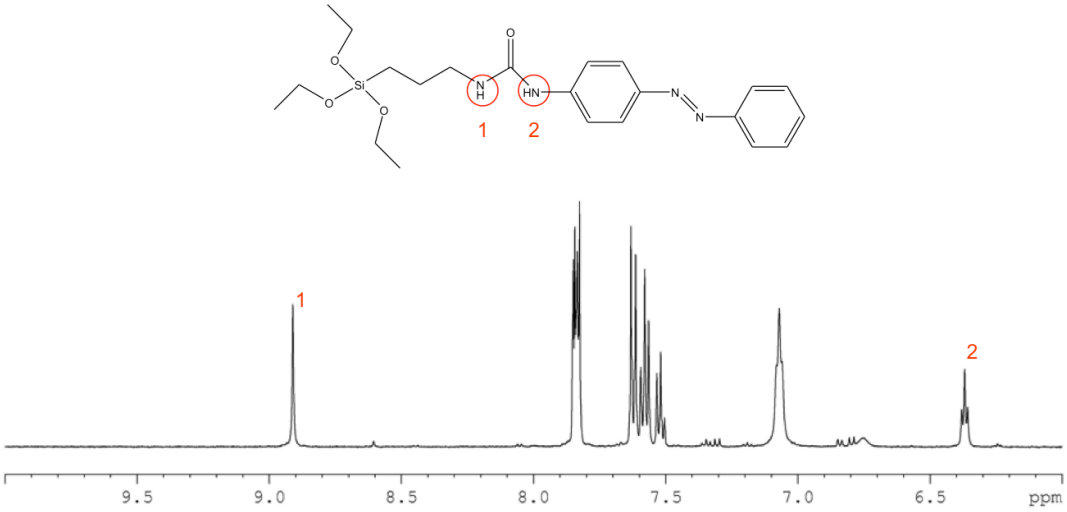

Figure 2.4. ^{1}H-NMR characterization of the coupled AzoH-ICPES in dimethyl sulfoxide (DMSO). The chemical shifts at $\delta = 8.91$ (marked as 1) and 6.37 (marked as 2) correspond to the urea H close to silane and the other urea H close to aryl. This data demonstrates that AzoH is coupled to the linker molecule in agreement with previous reports.[5,18]

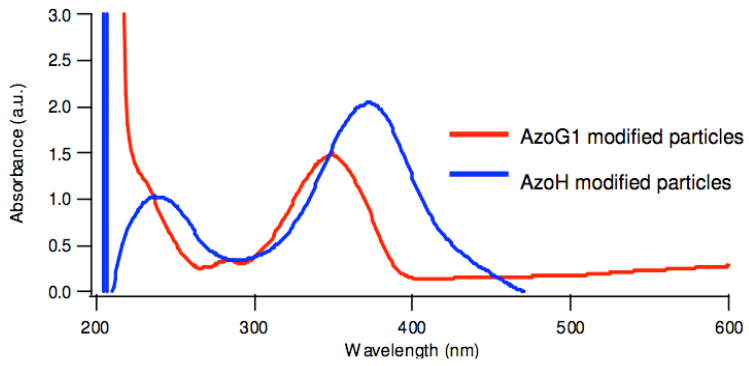

Figure 2.5. UV-Vis spectroscopy of azobenzene-modified particles. AzoH modified particles have been solvent extracted. The absorption peaks between 300 and 400 nm confirm that the particles are functionalized with azobenzene molecules.

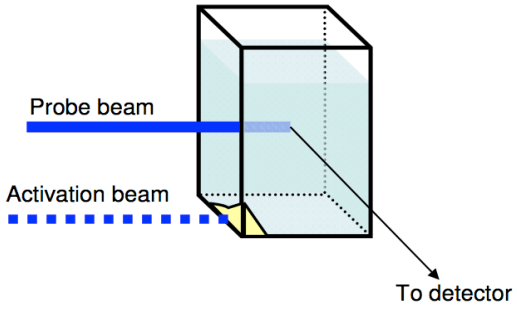

Figure 2.6. Spectroscopic setup for controlled release experiments. 15 mg of dye-loaded, azobenzene-functionalized particles are placed in the corner of a cuvette, and 12 mL of MeOH is added. A 1 mW, 457 nm probe beam directed into the liquid is used to excite the dissolved dye molecules. After several minutes, a 9 mW, 457 nm activation beam used to excite the azobenzenes' motion is turned on. The luminescence spectrum of the dissolved dye is collected in 1 second intervals over the course of the experiment. The release profiles are obtained by plotting the luminescence intensity at the emission maximum as a function of time.

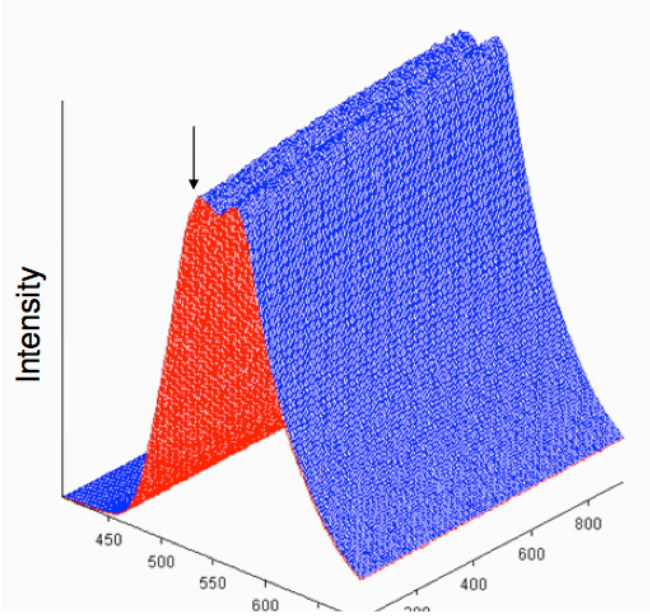

Figure 2.7. Plot of coumarin 540A emission as a function of time. The emission intensity at 540 nm is plotted vs time to obtain the release profile shown in Figure 2.8.

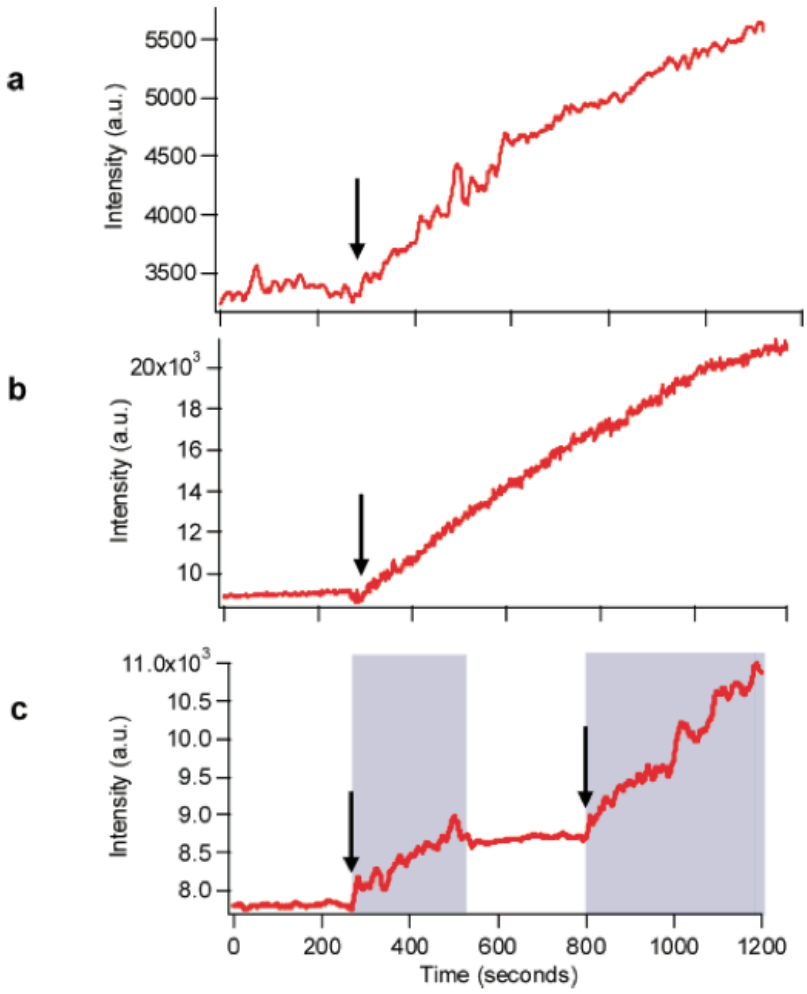

Figure 2.8. Plots of the luminescence intensity of C540A at 540 nm in solution as a function of time measured at 1 sec intervals. The arrows indicate when the azobenzene excitation light (457 nm) is turned on. Release profile of C540A from (a) AzoH-modified particles prepared by the CCM; (b,c) AzoG1 modified particles prepared by the PSMM. Profile (c) demonstrates the on-off response to 457 nm excitation. Shaded regions indicate periods of time at which the azobenzene excitation light is on.

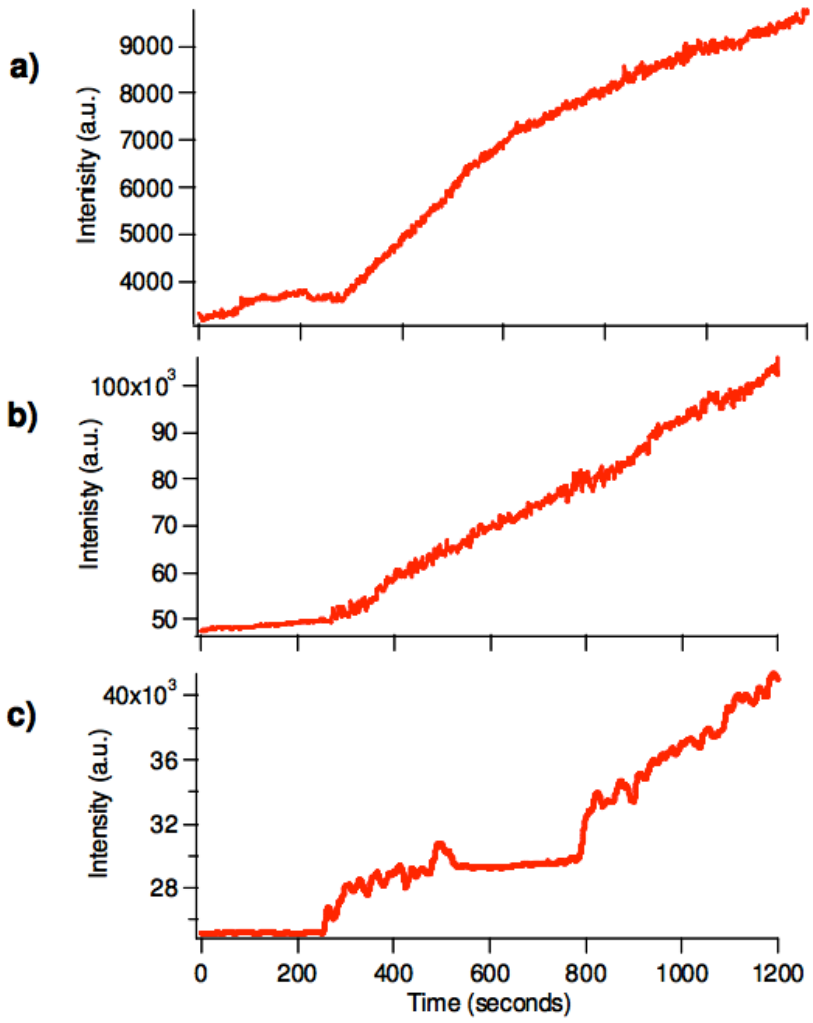

Figure 2.9. Rhodamine 6G release profiles from (a) AzoH-modified particles prepare by the CCM; (b,c) AzoG1-modified particles prepared by the PSMM. Profile (c) illustrates the on-off response to 457 nm excitation.

2.7. References

[1] J. S. B. C.T. Kresge, M.E. Leonowicz, W.J. Roth, J.C. Vartuli, *Nature* **1992**, *359*, 710–712.

[2] Y. Lu, R. Ganguli, C. Drewien, M. Anderson, J. I. Zink, *Nature* **1997**, *389*, 651–655.

[3] S. Huh, J. W. Wiench, J. Yoo, M. Pruski, V. S. Lin, *Chem. Mater.* **2003**, *15*, 4247–4256.

[4] N. Liu, Z. Chen, D. R. Dunphy, Y.-B. Jiang, R. A. Assink, C. J. Brinker, *Angew. Chem Int. Ed.* **2003**, *42*, 1731–4.

[5] A. Silsesquioxane, N. Liu, K. Yu, B. Smarsly, D. R. Dunphy, Y. Jiang, C. J. Brinker, **2002**, 14540–14541.

[6] N. Liu, D. R. Dunphy, P. Atanassov, S. D. Bunge, Z. Chen, G. P. Lo, T. J. Boyle, C. J. Brinker, *Nano Lett.* **2004**, *4*, 551–554.

[7] E. Besson, A. Mehdi, D. Lerner, C. Rey, R. J. P. Corriu, *J. Mater. Chem.* **2005**, *15*, 803.

[8] K. Weh, J. Caro, M. Noack, K. Hoffmann, K. Schr, **2002**, *54*, 15–26.

[9] M. Alvaro, M. Benitez, D. Das, H. Garcia, E. Peris, **2005**, 4958–4964.

[10] T. D. Nguyen, K. C.-F. Leung, M. Liong, C. D. Pentecost, J. F. Stoddart, J. I. Zink, *Org. Lett.* **2006**, *8*, 3363–6.

[11] T. D. Nguyen, H.-R. Tseng, P. C. Celestre, A. H. Flood, Y. Liu, J. F. Stoddart, J. I. Zink, *Proc. Natl. Acad. Sci. U. S. A.* **2005**, *102*, 10029–34.

[12] K. C. Leung, T. D. Nguyen, J. F. Stoddart, J. I. Zink, *Chem. Mater.* **2006**, *18*, 5919–5928.

[13] R. Hernandez, H.-R. Tseng, J. W. Wong, J. F. Stoddart, J. I. Zink, *J. Am. Chem. Soc.* **2004**, *126*, 3370–1.

[14] N. K. Mal, Y. Tanaka, *Nature* **2003**, *421*, 350–353.

[15] N. K. Mal, M. Fujiwara, Y. Tanaka, T. Taguchi, M. Matsukata, *Chem. Mater.* **2013**, *15*, 3385–3394.

[16] C.-Y. Lai, B. G. Trewyn, D. M. Jeftinija, K. Jeftinija, S. Xu, S. Jeftinija, V. S.-Y. Lin, *J. Am. Chem. Soc.* **2003**, *125*, 4451–9.

[17] P. Sierocki, H. Maas, P. Dragut, G. Richardt, F. Vögtle, L. De Cola, F. a M. Brouwer, J. I. Zink, *J. Phys. Chem. B* **2006**, *110*, 24390–8.

[18] N. Liu, D. R. Dunphy, M. a Rodriguez, S. Singer, J. Brinker, *Chem. Commun.* **2003**, 1144–5.

CHAPTER 3.

Light-Activated Nanoimpeller-Controlled Drug Release

in Cancer Cells

3.1. Abstract

In this chapter, nanoimpeller-based mesoporous silica particles is used to deliver molecules into living cells under photocontrol. Confocal microscope imaging of cells, containing the particles loaded with the membrane-impermeable dye, propidium iodide (PI) and the anticancer drug, camptothecin (CPT) respectively, shows that staining of the nuclei and cell apoptosis occur only when impellers are photoexcited to release the molecules.

3.2. Introduction

Nano-mechanical systems designed to trap and release molecules from pores in response to a stimulus are the subjects of intensive current investigation.[1-21] Such systems have potential applications for precise drug delivery. A photo-activated material, for example, could release a drug under external control only at a specific time and place for photo-therapy. Nano-materials suitable for this type of operation must consist of both an appropriate container and a photo-activated moving component.

Mesoporous silica made by sol-gel methods[22-24] is a very useful container for molecules because the pores of both particles[22,25] and films[23] are accessible to liquids and gases. The pores in the silica materials are formed by templating agents, usually surfactants, that are removed after the formation structure was completed.[22,23] Diffusion of molecules driven by concentration gradients, including biomolecules, into and out of the pores has been demonstrated.[26] Methods have been developed to make tubular pores whose inner diameters can be varied between about 1-10 nm.[27] The pore walls and silica frameworks can be readily derivatized with a large variety of molecules.[28-30] Mesoporous silica nanoparticles with an average diameter of about 200 nm

can enter cells and have been used as gene transfection reagents, cell markers, and carriers of molecules such as drugs and proteins.[5,31-37]

Photo-activated moving parts based on the photoisomerization of azobenene derivatives have been used in conjunction with mesoporous silica.[9-13] The dynamics of the motion in pores of derivatives with substituents ranging from hydrogens to dendrimers has been studied.[38] The decrease in the size of trans to cis isomers of azobenzenes attached to pore interiors has been used to regulate the transport of molecules through pores to electrodes.[13] In the previous chapter, the back and forth wagging motion was demonstrated to act a molecular impeller that regulates the release of molecules from the pores of silica nanoparticles under "remote control" upon photoexcitation.[9,14] Azobenzene driven release, unlike that regulated by many other nanomachines, can occur in aqueous environments.

A second category of molecular machines, called nanovalves, have been made by attaching various caps and molecular moving parts to the pore entrances to control the entrance and egress of molecules into and from the pores. Examples of caps include coumarin dimers,[7-9] CdS[5] or gold[6]-nanoparticles, polymeric gels,[1-3] and a gold membrane.[4] Valves based on moving parts that respond to external stimuli have been demonstrated including trapping and releasing of molecules by pH,[17] redox,[16] and competitive binding.[15] A completely reversible nanovalve that can be opened and closed at will has been used to control release of molecules from ~2 nm pores of mesoporous silica nanoparticles.[16] Examples of non-valved light-controlled release include photosensitive liposomes[39-42] and liposomes containing gold particles heated by photoexcitation,[43] but only one type of valve actuated by light has been reported.[18] Currently, the majority of these valves (including the light-driven valve) only function in organic

solvents because the supramolecular recognition and binding motifs are disrupted by highly polar and hydrogen bonding solvents such as water.

This chapter demonstrates the use of nanoimpeller-controlled mesostructured silica nanoparticles to deliver and release anticancer drugs into living cells upon external command. By using light-activated mesostructured silica (LAMS) nanoparticles, luminescent dyes and anticancer drugs are only released inside of cancer cells that are illuminated at the specific wavelengths that activate the impellers. The quantity of molecules released is governed by the light intensity and the irradiation time. Human cancer cells (a pancreatic cancer cell line, PANC-1 and a colon cancer cell line, SW 480) were exposed to suspensions of the particles and the particles were taken up by the cells. Confocal microscopy imaging of cells containing the particles loaded with the membrane-impermeable dye, propidium iodide (PI), shows that the PI is released from the particles only when the impellers are photoexcited (~ 0.1 W/cm^2), resulting in staining of the nuclei. The anticancer drug camptothecin (CPT) was also loaded into and released from the particles inside the cells under light excitation, and apoptosis was induced. Intracellular release of molecules is sensitively controlled by the light intensity, irradiation time, and wavelength, and the anticancer drug delivery inside of cells is regulated under external control.

3.3. Results and Discussion

3.3.1. Synthesis and characterization of the LAMS

The LAMS functionalized with azobenzene molecules were synthesized using modifications of reported processes.[12,14] In attempt to accomplish the complete trap of the cargo molecules in the particles before the light stimuli, a smaller pore (~ 1.8 nm) was templated by using the cationic surfactant dodecyltrimethylammonium bromide (DTAB) having a shorter chain length. In the resulting particles, azobenzene moieties were positioned in the pore interiors with one end attached to the pore walls and the other end free to undergo photoisomerization (Figure 3.1). The morphology of the spherical particles with ordered arrays of the pores was proven by scanning electron microscopy (SEM) and transmission electron microscopy (TEM) (Figure 3.2). The X-ray diffraction pattern exhibited a strong Bragg peak indexed as {100} at $2\theta = 2.43°$, corresponding to a d-spacing of ~ 3.6 nm. Analysis on the nitrogen sorption isotherm of the particles taken at 77 K indicated the BJH average pore diameter of 1.9 ± 0.1 nm, BET surface area of 621.19 $m^2 g^{-1}$, and total pore volume of 0.248 $cm^3 g^{-1}$. It was calculated from UV/Vis spectroscopy that the silica particles contain about 2.4 wt % of the azobenzene derivatives.

3.3.2. Photo-controlled release of Rhodamine B dye in aqueous solution

Controlled expulsion of the pore contents into solution was monitored by luminescence spectroscopy.[14] Hydrophilic Rhodamine B was chosen as a probe dye to verify that the moving parts are able to trap and release the probe molecules in an aqueous environment. The fluorescence emission spectrum of the Rhodamine B probe molecules that were released from the particles into water was recorded at one second intervals. The intensities at the emission maximum (λ ~ 575 nm) as a function of time are plotted in Figure 3.3. The impellers in the nanopores trap the probe molecules in the dark and

promptly release them in response to the light excitation. When a larger pore (~ 2 nm in diameter) templated from the CTAB surfactant was tested in the same experiment, a little leakage of the system was observed in the dark (Figure 3.4).

3.3.3. Photo-controlled release of molecules in living cells

3.3.3.1. Staining of cell nuclei by PI dye

Based on the successful operation of the impeller in water, *in vitro* studies were carried out on two human cancer cell lines (PANC-1 and SW480). To detect the photo-responsive behavior of the impellers inside of cells, a membrane-impermeable dye, PI was chosen as the fluorescent probe molecule and loaded into the particles following the same procedure as that used for the Rhodamine B loading. The cells were cultured overnight on a Lab-Tek chamber slide system (Nalge Nunc International). After 3 h of incubation in the dark with a 10 μg/mL homogeneous suspension of PI-loaded LAMS containing ~ 0.24 μg of the azobenzene machines, the cells were irradiated at 413 nm, a wavelength at which both *cis* and *trans* azobebenzene isomers have almost the same extinction coefficient. The cells were exposed to three different excitation fluences (~ 0.01, 0.1, 0.2 W/cm^2) with exposure times ranging from 0 to 5 min. As a control, the cells were also exposed to 676 nm, a wavelength at which azobenzene does not absorb, at the same light intensities for the same amounts of time as in the release experiments. After irradiation, the cells were again incubated in the dark for 10 min to allow the released PI to stain the nuclei of the cells, and then examined by confocal microscopy (λ_{ex} = 337 nm; Carl Zeiss LSM 310 Laser Scanning Confocal microscope).

Confocal fluorescence images of the PANC-1 cells showed that only after the photo-activation of the azobenzene impellers was the PI released from the LAMS, resulting in staining of the cell nuclei (Figure 3.5). When the cells were irradiated for 5 min with 413 nm light of ~ 0.2 W/cm^2 beam intensity, the nuclei were dyed red, but negligible dying of the nuclei was observed in the cells kept in the dark. For cells excited with a decreased intensity, ~ 0.1 W/cm^2, the nuclei were stained to a lighter red, and no staining was observed from ~ 0.01 W/cm^2 irradiation, which did not activate the impellers enough to enable them release much PI (Figure 3.5.A (d-f)). When exposed to different excitation times of up to 5 min under constant fluence of ~ 0.2 W/cm^2 at 413 nm, the nuclei were stained increasingly redder with increasing activation time (Figure 3.5.A (a-c, f)), verifying that the amount of PI released is directly related to the total number of photons absorbed. The cells were not stained when the LAMS were irradiated at 676 nm (~ 0.2 W/cm^2) because that wavelength is not absorbed by the impellers (Figure 3.5.C). These results prove that the impeller operation can be regulated by the light intensity, excitation time, and specific wavelength, and that these controllable factors directly affect the amount of the pores' contents that is released. When cells were incubated with free PI that were not loaded into the particles, cell staining did not occur (Figure 3.5.B (h)), proving that the free PI molecules cannot enter the cells. The staining of the nuclei is thus caused only by the PI that is carried into the cells by the LAMS and released from the particles when they are photoexcited. Similar results were obtained in experiments using colon cancer cells SW480 (Figure 3.6). Staining of the nuclei was caused by illuminating the LAMS with ~ 0.2 W/cm^2, 413 nm light. The LAMS particles function controllably in multiple cell types.

3.3.3.2. Cell apoptosis by CPT anticancer drug

To test the ability of the LAMS to transport and then controllably release drug molecules inside cancer cells, the particles were loaded with the anticancer drug camptothecin (CPT). A homogeneous suspension of 10 μg/mL of the drug-loaded particles was added to the cancer cells. After 3 hours of incubation in the dark were irradiated with ~ 0.1 W/cm^2, 413 nm light for various excitation times (0 to 10 min). The power density of ~ 0.1 W/cm^2 was chosen for this experiment based on the PI cell staining results. For the confocal cell imaging measurements, the irradiated cells were again incubated for 48 h in the dark and then stained with a 1:1 mixture solution of PI and Hoechst 33342 dye to investigate the cell death. As control experiments, cells incubated with empty LAMS particles and cells without any treatment were exposed to the excitation light.

Cell death was induced under photocontrol. In the absence of light excitation, the CPT remained in the particles and the cells were not damaged (Figure 3.7.C (l)). Illumination, however, promptly expelled the CPT from the particles, causing cancer cell apoptosis that is demonstrated by nuclear fragmentation and chromatin condensation (Figure 3.7.A). The cell nuclei all fluoresced blue from the Hoechst 33342 dye while no red fluorescent cell nuclei stained by the PI dye were detected, confirming that the cell death did not result from cellular membrane damage but from apoptosis by the released CPT inside of the cells. The cells containing empty LAMS particles (no CPT) that were exposed to the excitation beam for 10 min did not undergo cell death, indicating that the LAMS particles are biocompatible with the living cells (Figure 3.7.B (h, i)). The ~ 0.1 W/cm^2, 413

nm activation light beam did not affect the cell survival (Figure 3.7.B (g)). CPT suspended in PBS was not taken up by the cells due to its insolubility and thus did not kill the cells. These observations demonstrate that cancer cell apoptosis is caused only by the CPT released from the LAMS particles inside cells under external photocontrol.

To further confirm that cell death was caused by the cytotoxicity of the CPT expelled from the particles, quantitative measurements of cell viability were made for another set of the same samples (10 μg/mL particles incubated with cells) placed in 96-well plates. After incubation with LAMS with and without CPT loaded and illumination with ~ 0.1 W/cm2, 413 nm light, the cells were kept in the incubator for an additional 72 hours. The number of surviving cells was then counted using a cell counting kit from Dojindo Molecular Technologies, Inc.[37] The results showed that the cell death induced by CPT induced by CPT only occurred under light illumination, an the cell death rate increases with longer cell illumination time, which is consistent with the cell morphologic observations. The surviving cells decreased to about half after 10 min of photoexcitation of the impellers (Figure 3.8). At a higher concentration (100 μg/mL) of the particles, cell survival decreased more dramatically; only ~ 40 % of the PANC-1 cells and ~ 14 % of the SW480 survived the released CPT after 10 min of light excitation (Figure 3.8).

3.4. Summary

In summary, it was demonstrated that the biocompatible nanoimpeller-based delivery system regulates the release of molecules from the nanoparticles inside of living cells. This nanoimpeller system may open a new avenue for drug delivery under external

control at a specific time and location for photo-therapy. Manipulation of the machine is achieved by remote control by varying both the intensity of the light and time that the particles are irradiated at the specific wavelengths where the azobenzene impellers absorb. The CPT loading (~ 0.6 wt %) in the LAMS was higher than that for underivatized mesostructured silica (~ 0.06 wt %), possibly because of the hydrophobic molecular interactions between azobenzene moieties and CPT. When excited at 413 nm, the azobenzenes' continuous photoisomerization acts as an impeller and expels CPT out of the pores. The light intensity needed to activate the impellers, ~ 0.1 W/cm^2 at 413 nm, does not damage the cells. The action of the LAMS is monitored by release of PI and the consequent staining of the cell nuclei, and by the release of CPT that induces apoptosis. The delivery and release capability of light-activated mesostructured silica particles containing molecular impellers is the first step towards a novel platform for the next generation of nanotherapeutics with both spatial and temporal external control.

3.5. Experimental Section

3.5.1. Synthesis of light-activated mesostructured silica nanoparticles

The chemicals for the particle synthesis were purchased from Sigma-Aldrich. The bifunctional modification strategy[29,30] was used to incorporate 4-phenylazoaniline (4-PAA) into the interiors of the particle pores. Organosilane molecules containing azobenzene moieties were first generated via coupling reaction of 0.142 g of the 4-PAA with 0.71 mL of the isocyanatopropylethoxysilane (ICPES) linker in 5 mL ethanol under N_2 for 4 hours.

In another flask, 1g of the templating agent dodecyltrimethylammonium bromide (DTAB), 3.5 mL of 2M NaOH, and 480 g of deionized H_2O were stirred for 30 min at 80ºC. To this surfactant solution, 4.67 g of the tetraethylorthosilicate (TEOS) and the ethanol solution containing the azobenzene machines were slowly added and vigorously stirred. After 2 h the particles were filtered and washed with MeOH. The surfactant was extracted by stirring 1 g of the particles in 100 mL of MeOH with 1 mL of concentrated HCl solution for 6 h at 60 ºC.

3.5.2. Dye loading procedure

The probe molecules, Rhodamine B or propidium iodide, are loaded into the mesopores by soaking and stirring ~ 20 mg of the particles in a 1 mM aqueous solution of the dye at room temperature for 12 h. Then the particle suspensions in aqueous dye solution were centrifuged ~ 10 min, supernatant solution was taken out, and the centrifuged particles were again suspended in deionized water; this step was repeated at least twice to thoroughly remove the dyes adsorbed onto the particle surface, and then the washed particles were dried at room temperature.

3.5.3. Anticancer drug loading procedure

A solution of 0.6 mL dimethylsulfoxide (DMSO) containing 1 mg of the CPT molecules was prepared, and 10 mg of the LAMS was added. After stirring the suspension for 24 h, the mixture was centrifuged for 10 min and the supernatant solution removed. The CPT-loaded LAMS were then dried under vacuum. To determine the amount of CPT

molecules loaded in the LAMS, the drug-loaded LAMS were dissolved and sonicated with 4 mL DMSO, placed in a quartz cuvette as in the release experiment, and irradiated by ~ 0.2 W/cm^2, 413 nm light for 10 min. The DMSO suspension of the particles was then centrifuged and the UV/Vis absorption spectrum of supernatant solution containing the released CPT molecules was measured. The concentration of CPT calculated from the absorbance was ~ 0.09 mM. To confirm that most of the loaded CPT molecules were released from the particles, the supernatant taken out for the absorbance measurement was placed back into the cuvette with the centrifuged particles, excited for 50 min, and the absorbance measurement was repeated. It was determined that about 0.12 mg of CPT molecules was loaded into 20 mg of the particles.

3.5.4. Spectroscopic setup for controlled release experiments

The Rhodamine B-loaded particles were carefully placed on the bottom of a cuvette filled with deionized H_2O. The liquid above powder was monitored continuously by a 10 mW, 530 nm probe beam. The LAMS powder was activated with a 10 mW, 457 nm excitation beam. Both the cis and trans azobenzene isomers absorb at that wavelength with a conversion quantum yield of about 0.4 for trans to cis and 0.6 for cis to trans.[38] The release profiles are obtained by plotting the luminescence intensity at the emission maximum as a function of time.

3.5.5. Cell culture

PANC-1 and SW480 Cells were obtained from the American Type Culture Collection and were maintained in Dulbecco's modified Eagle's medium (DMEM) (GIBCO) and Leibovitz's L-15 medium (Cellgro) respectively, supplemented with 10% fetal calf serum (Sigma, MO), 2% L-glutamine, 1% penicillin, and 1% streptomycin stock solutions with regular passage.

3.5.6. Cell death assay

Cell death was also examined by using the propidium iodide and Hoechst 33342 double-staining method. The cells incubated on a Lab-Tek chamber slide system were stained with propidium iodide/Hoechst 33342 (1:1) for 5 min after treatment with CPT-loaded LAMS or free LAMS followed by light irradiation, and then examined with fluorescence microscopy. The cell survival assay was performed by using the cell-counting kit from Dojindo Molecular Technologies, Inc. Cancer cells were seeded in 96-well plates (5000 cells/well) and incubated in fresh culture medium at 37 ^{o}C in a 5 % CO_2/ 95 % air atmosphere for 24 h. After incubation with LAMS with and without CPT loaded and illumination with ~ 0.1 W/cm^2, 413 nm light, the cells were kept in the incubator for an additional 72 h. The cells were then washed with PBS and incubated in DMEM with 10 % WST-8 solution for another 2 h. The absorbance of each well was measured at 450 nm with a plate reader. Since the absorbance is proportional to the number of viable cells in the medium, the viable cell number was determined by using a previously prepared calibration curve (Dojindo Co.).

3.5.7. Statistical analysis

All results are expressed as mean values the standard deviation (SD). Statistical comparisons were made by using Student's t-test after analysis of variance. The results were considered to be significantly different at a P value < 0.05.

3.6. Figures

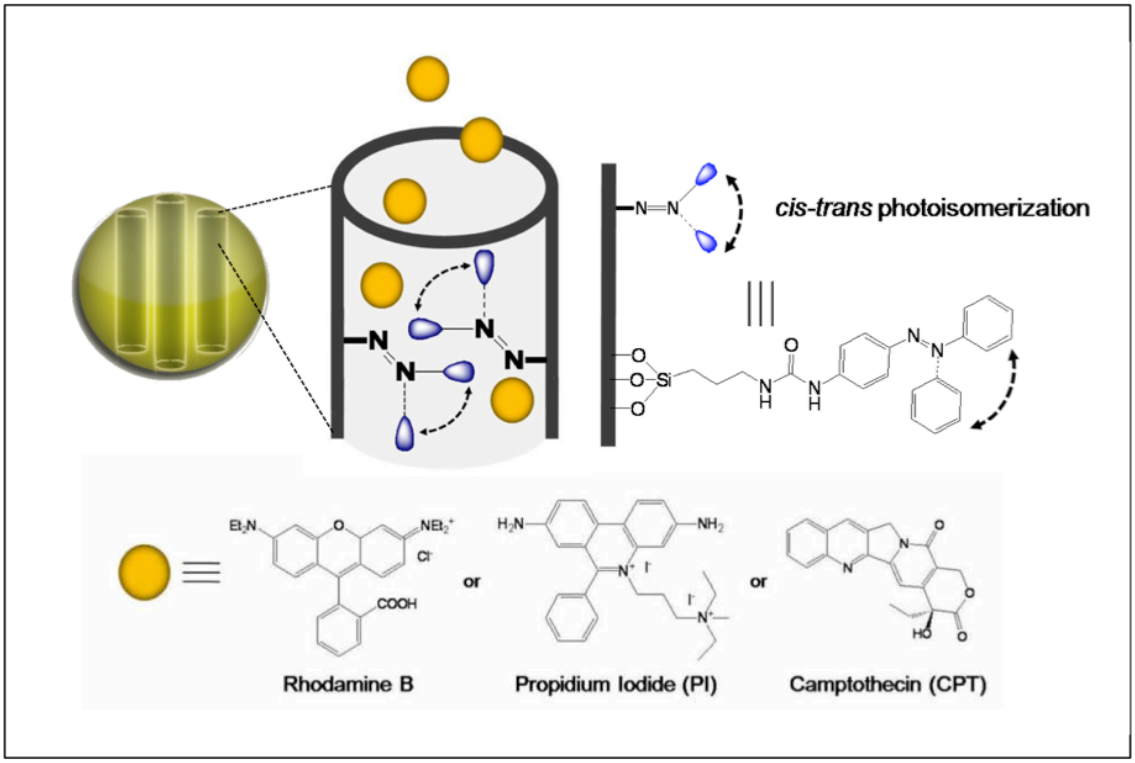

Figure 3.1. Designed pore interiors of the light-activated mesostructured silica nanoparticles (LAMS) functionalized with azobenzene derivatives. Continuous illumination at 413 nm causes a constant trans-cis photoisomerization about the N=N bond causing dynamic wagging motion of the azobenzene derivatives and results in the release of the molecules in, through, and out of the mesopores.

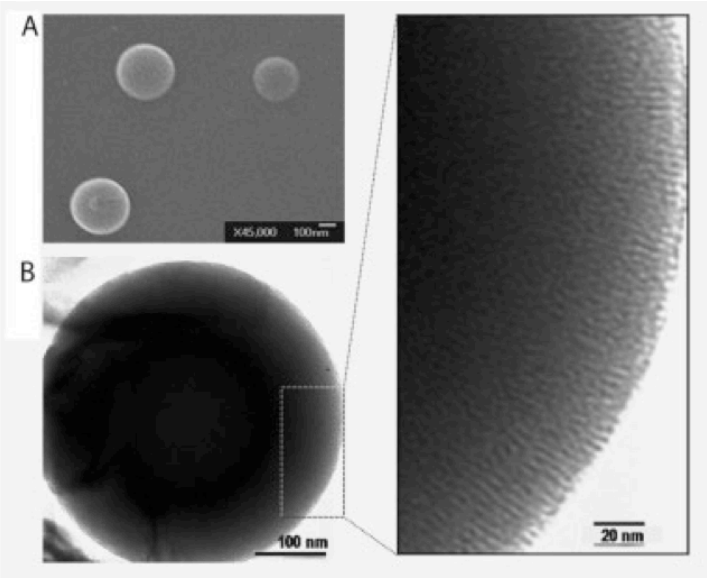

Figure 3.2. Characterization of the surfactant-extracted LAMS particles. (A) scanning electron microscopy (SEM) and (B) transmission electron microscopy (TEM) images of the particles. Right: maginified portion of TEM image. The pores can be seen.

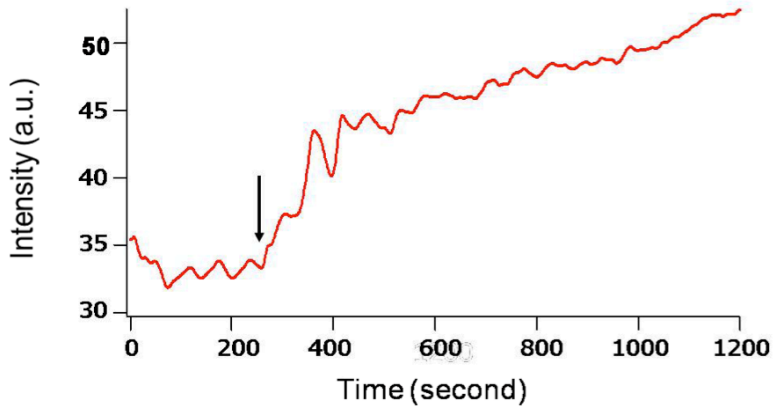

Figure 3.3. Time-dependent release of Rhodamine B dye from the photoexcited particles into water. The arrow indicates the time at which the azobenzene activation light was turned on.

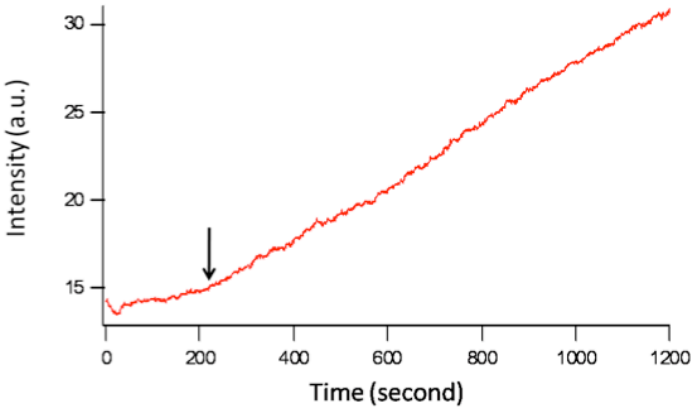

Figure 3.4. Release of Rhodamin B dye molecules from the larger pores (~ 2 nm) of the LAMS templated by cetyltrimethylammonium bromide (CTAB) surfactant.

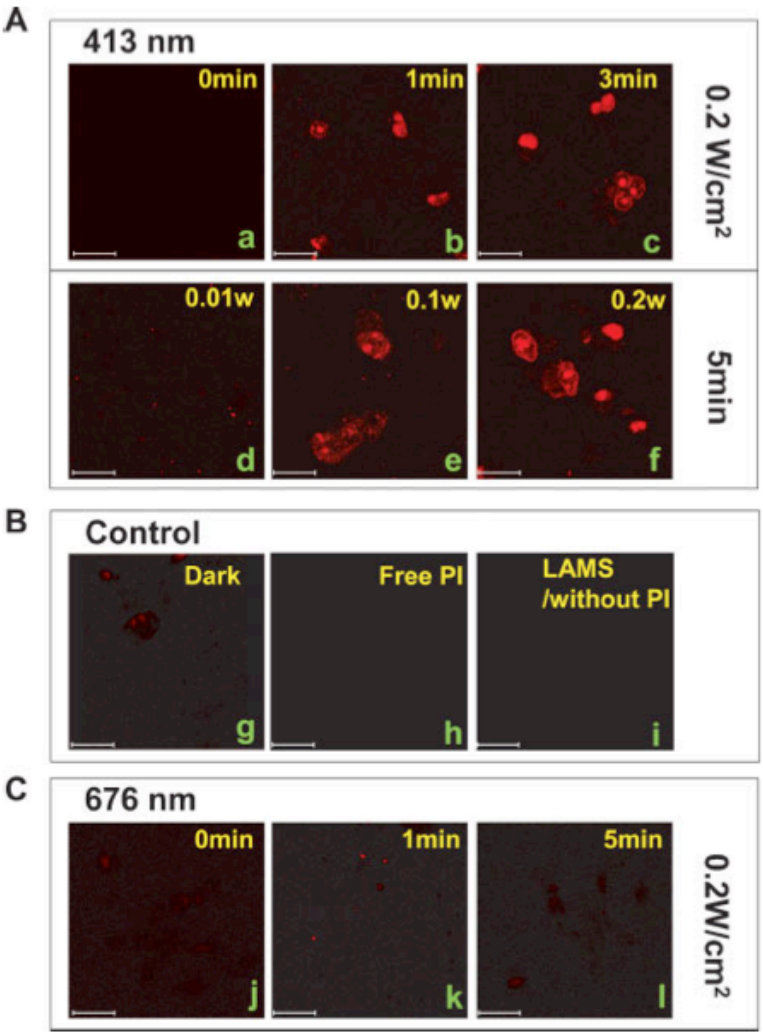

Figure 3.5. Confocal microscope images of the photocontrolled staining of the nuclei of PANC-1 cancer cells. Plasma membrane impermeable propidium iodide (PI) molecules were loaded in the pores of LAMS and the dye loaded particles were incubated with the cells for 3 hours in the dark. The cells were then exposed to the activation beam for 1 to 10 min. After further incubation in the dark for 10 min, the cells were examined with confocal microscopy (λex = 337 nm) A. Cells incubated with the PI-loaded LAMS and illuminated for 0 (a), 1 (b), 3 (c), or 5 min (f) under a constant ~ 0.2 W/cm^2, 413 nm light or with

different light intensities (~ 0.01 (d) or ~ 0.1 W/cm^2 (e) for 5 min at a 413 nm light). B. PANC-1 cells incubated with the PI-loaded LAMS (g), free PI molecules (h), or empty LAMS (i) were kept in the dark and exposed to a 413 nm light. C. Cells incubated with the PI-loaded LAMS were illuminated with ~ 0.2 W/cm^2, 676 nm light for 0 (j), 1 (k) or 5 min (l).

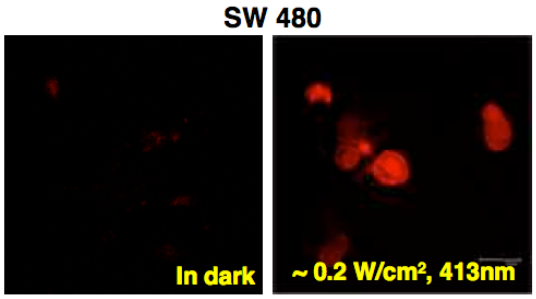

Figure 3.6. Confocal microscope images of the photocontrolled staining of the nuclei of SW480 cancer cells. Propidium iodide molecules were loaded in the pores of LAMS and the dye-loaded particles were incubated with the cells for 3 h in the dark. The cells were then exposed to the 0.2 W/cm^2, 413 nm activation beam for 5 min (right) or kept in the dark (left). After further incubation in the dark for 10 min, confocal microscopy (λex = 337 nm) showed that propidium iodide stained the nuclei of only the irradiated cells.

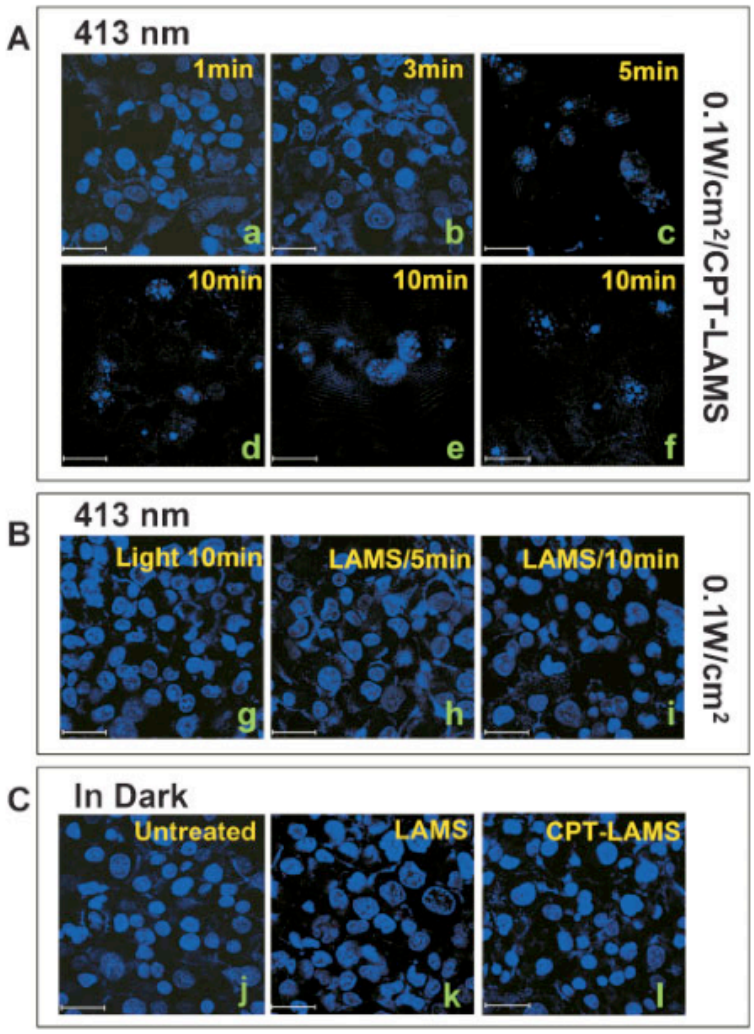

Figure 3.7. Light-triggered delivery of the anticancer drug camptothecin (CPT) inside PANC-1 cancer cells to induce apoptosis. CPT molecules were loaded into the pores of the LAMS and a homogeneous suspension of the CPT-loaded particles (10 mg/ml) was added to the cells which were incubated in Lab-Tek chamber slides for 3 h in dark. The cells were then irradiated under ~ 0.1 W/cm^2, 413 nm light for 1 to 10 min, again incubated in the dark for 48 h, and double-stained with propidium iodide/Hoechst 33342 solution (1:1). A. CPT-loaded particles were incubated with cancer cells and illuminated for 1 (a), 3 (b), 5 (c)

or 10 min (d, e, f). B. As controls, pure cells (no particles) were exposed to the light for 10 min (g), and cells including the CPT-unloaded LAMS were exposed for 5 (h) or 10 min (i). C. Untreated pure cells (j), cells incubated with CPT-unloaded (k) or -loaded (l) LAMS were kept in the dark for 48 h.

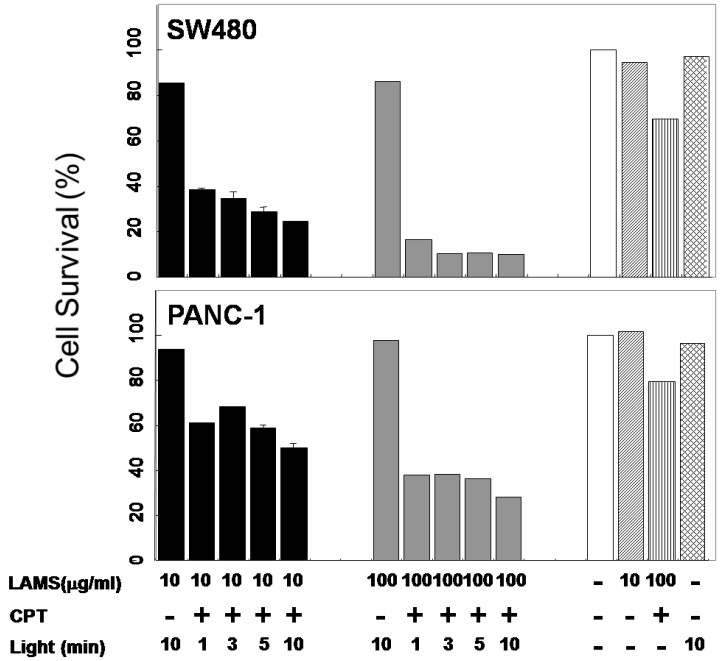

Figure 3.8. In vitro cytotoxicity assay. 5000 PANC-1 or SW480 cancer cells were incubated with different concentrations of CPT-loaded or unloaded particles in 96 well cell culture plates. After incubation for 72 h following the light excitation, the numbers of surviving cells were counted using the cell counting kit. The viability is shown as the percentage of the viable cell number in treated wells compared to untreated wells. All experiments were performed in triplicate, and the results are shown as means ± SD. LAMS: cells treated with the LAMS of 10 or 100 mg/ml. CPT: CPT was loaded (+) or absent in the LAMS. Light: cells were exposed to blue light (wavelength 413 nm) for 0, 1, 3, 5 or 10 min, followed by incubation for 72 h.

3.7. References

[1] Q. Fu, G. V. R. Rao, L. K. Ista, Y. Wu, B. P. Andrzejewski, L. A. Sklar, T. L. Ward, G. P. Lopez, *Adv. Mater.*, **2003**, *15*, 1262.

[2] I. C. Kwon, Y. H. Bae, S. W. Kim, *Nature*, **1991**, *354*, 291.

[3] W. E. Rudzinski, T. Chipuk, A. M. Dave, S. G. Kumbar, T. M. Aminabhavi, *J. Appl. Poly. Sci.*, **2003**, *87*, 394.

[4] J. T. Santini, M. J. Cima, R. Langer, *Nature*, **1999**, *397*, 335.

[5] C. Y. Lai, B. G. Trewyn, D. M. Jeftinija, K. Jeftinija, S. Xu, S. Jeftinija, V. S. Y. Lin, *J. Am. Chem. Soc.*, **2003**, *125*, 4451.

[6] F. Torney, B. G. Trewyn, V. S. Y. Lin, K. Wang, *Nature Nanotech.*, **2007**, *2*, 295.

[7] N. K. Mal, M. Fujiwara, Y. Tanaka, *Nature*, **2003**, *421*, 350.

[8] N. K. Mal, M. Fujiwara, Y. Tanaka, T. Taguchi, M. Matsukata, *Chem. Mater.*, **2003**, *15*, 3385.

[9] Y. Zhu, M. Fujiwara, *Angew. Chem. Int. Ed. Engl.*, **2007**, *46*, 2241.

[10] M. Alvaro, M. Benitez, D. Das, H. Garcia, E. Peris, *Chem. Mater.*, **2005**, *17*, 4958.

[11] N. Liu, K. Yu, B. Smarsly, D. R. Dunphy, Y. B. Jiang, C. J. Brinker, *J. Am. Chem. Soc.*, **2002**, *124*, 14540.

[12] N. Liu, Z. Chen, D. R. Dunphy, Y. B. Jiang, R. A. Assink, C. J. Brinker, *Angew. Chem. Int. Ed. Engl.*, **2003**, *42*, 1731.

[13] N. G. Liu, D. R. Dunphy, P. Atanassov, S. D. Bunge, Z. Chen, G. P. Lopez, T. J. Boyle, C. J. Brinker, *Nano Lett.*, **2004**, *4*, 551.

[14] S. Angelos, E. Choi, F. Vogtle, L. DeCola, J. I. Zink, *J. Phys. Chem. C*, **2007**, *111*, 6589.

[15] K. C. F. Leung, T. D. Nguyen, J. F. Stoddart, J. I. Zink, *Chem. Mater.*, **2006**, *18*, 5919.

[16] T. D. Nguyen, H. R. Tseng, P. C. Celestre, A. H. Flood, Y. Liu, J. F. Stoddart, J. I. Zink, *Proc. Natl. Acad. Sci. U.S.A.*, **2005**, *102*, 10029.

[17] T. D. Nguyen, K. C. F. Leung, M. Liong, C. D. Pentecost, J. F. Stoddart, J. I. Zink, *Org. Lett.*, **2006**, *8*, 3363.

[18] T. D. Nguyen, K. C. F. Leung, M. Liong, Y. Liu, J. F. Stoddart, J. I. Zink, *Adv. Func. Mater.*, **2007**, *17*, 2101.

[19] T. D. Nguyen, Y. Liu, S. Saha, K. C. F. Leung, J. F. Stoddart, J. I. Zink, *J. Am. Chem. Soc.*, **2007**, *129*, 626.

[20] S. Saha, K. C. F. Leung, T. D. Nguyen, J. F. Stoddart, J. I. Zink, *Advanced Functional Materials*, **2007**, *17*, 685.

[21] S. Angelos, E. Johansson, J. F. Stoddart, J. I. Zink, *Adv. Func. Mater.*, **2007**, *17*, 2261.

[22] C. T. Kresge, M. E. Leonowicz, W. J. Roth, J. C. Vartuli, J. S. Beck, *Nature*, **1992**, *359*, 0028.

[23] Y. Lu, R. Ganguli, C. A. Drewien, M. T. Anderson, C. J. Brinker, W. Gong, Y. Guo, H. Soyez, B. Dunn, M. H. Huang, J. I. Zink, *Nature*, **1997**, *389*, 364.

[24] M. H. Huang, B. S. Dunn, H. Soyez, J. I. Zink, *Langmuir*, **1998**, *14*, 7331.

[25] S. Huh, J. W. Wiench, J. C. Yoo, M. Pruski, V. S. Y. Lin, *Chem. Mater.*, **2003**, *15*, 4247.

[26] Y. J. Han, G. D. Stucky, A. Butler, *J. Am. Chem. Soc.*, **1999**, *121*, 9897.

[27] J. S. Beck, J. C. Vartuli, W. J. Roth, M. E. Leonowicz, C. T. Kresge, K. D. Schmitt, C. T. W. Chu, D. H. Olson, E. W. Sheppard, S. B. McCullen, J. B. Higgins, J. L. Schlenkert, *J. Am. Chem. Soc.*, **1992**, *114*, 10834

[28] R. Hernandez, A. C. Franville, P. Minoofar, B. Dunn, J. I. Zink, *J Am Chem Soc*, **2001**, *123*, 1248.

[29] P. N. Minoofar, B. S. Dunn, J. I. Zink, *J. Am. Chem. Soc.*, **2005**, *127*, 2656.

[30] P. N. Minoofar, R. Hernandez, S. Chia, B. Dunn, J. I. Zink, A. C. Franville, *J Am Chem Soc*, **2002**, *124*, 14388.

[31] Y. S. Lin, C. P. Tsai, H. Y. Huang, C. T. Kuo, Y. Hung, D. M. Huang, Y. C. Chen, C. Y. Mou, *Chem. Mater.*, **2005**, *17*, 4570.

[32] D. R. Radu, C. Y. Lai, K. Jeftinija, E. W. Rowe, S. Jeftinija, V. S. Y. Lin, *J. Am. Chem. Soc.*, **2004**, *126*, 13216.

[33] Slowing, II, B. G. Trewyn, V. S. Lin, *J Am Chem Soc*, **2007**, *129*, 8845.

[34] M. Arruebo, M. Galan, N. Navascues, C. Tellez, C. Marquina, M. R. Ibarra, J. Santamaria, *Chem. Mater.*, **2006**, *18*, 1911.

[35] K. Weh, M. Noack, K. Hoffmann, K. P. Schroder, J. Caro, *Microporous Mesoporous Mater.*, **2002**, *54*, 15.

[36] E. Besson, A. Mehdi, D. A. Lerner, C. Reye, R. J. P. Corriu, *J. Mater. Chem.*, **2005**, *15*, 803.

[37] J. Lu, M. Liong, J. I. Zink, F. Tamanoi, *Small*, **2007**, *3*, 1341.

[38] P. Sierocki, H. Maas, P. Dragut, G. Richardt, F. Vogtle, L. D. Cola, F. A. Brouwer, J. I. Zink, *J. Phys. Chem. B*, **2006**, *110*, 24390.

[39] R. Schneider, L. Tirand, C. Frochot, R. Vanderesse, N. Thomas, J. Gravier, F. Guillemin, M. Barberi-Heyob, *Anticancer Agents Med. Chem.*, **2006**, *6*, 469.

[40] S. Ebrahim, G. A. Peyman, P. J. Lee, *Surv. Ophthalmol.*, **2005**, *50*, 167.

[41] T. Spratt, B. Bondurant, D. F. O'Brien, *Biochim. Biophys. Acta.*, **2003**, *1611*, 35.

[42] B. Bondurant, A. Mueller, D. F. O'Brien, *Biochim. Biophys. Acta.*, **2001**, *1511*, 113.

[43] L. Paasonen, T. Laaksonen, C. Johans, M. Yliperttula, K. Kontturi, A. Urtti, *J. Control Release*, **2007**, *122*, 86.

CHAPTER 4.

Drug Release from Three-Dimensional Cubic Mesoporous Silica Nanoparticles Controlled by Nanoimpellers

4.1. Abstract

Mesoporous silica nanoparticles with a cubic (*Ia*3*d*) pore structure are derivatized with light-activated nanoimpellers to control the release of loaded guest molecules under external photo-control. The nanoimpellers consist of azobenzene derivatives that are attached to the interiors of the three-dimensional interconnected pores, and undergo photoiosmerization that results in dynamic wagging motions of the unbound termini and drives the expulsion of molecules from the pores. Stimulated release experiments monitored by fluorescence spectroscopy demonstrate that the nanoimpeller-functionalized MCM-48 particles are able to trap and release both hydrophilic and hydrophobic cargo molecules under external photocontrol in aqueous, non-aqueous, and intracellular environments.

4.2. Introduction

Development of mechanized nanosystems that trap and release molecules in response to a specific stimulus is of current interest of researchers in the field of drug delivery. Nanoparticles of MCM-41,[1,2] a form of mesoporous silica possessing a well-ordered hexagonal array of tubular pores, have been extensively used as molecular containers [3–8] for constructing controlled release systems because of the high surface area, the large pore volume, and easy modification of the size and the surface composition of the pores. In conjunction with MCM-41 nanoparticles, recently devised controlled release systems have included a wide range of molecular machines[3,8–13] that are activated by external stimuli such as light,[14–21] pH changes,[22–26] competitive binding,[27] redox chemical energy,[28] magnetism,[29,30] and heat.[31] When the machines are stimulated by each source, guest molecules stored in the mesopores are promptly

released from the particles. These on-demand release systems have potential applications for precise *in vivo* drug delivery.

In the family of the mesoporous silica, another material, MCM-48[32,33] has a unique internal structure consisting of enatiomeric pairs of tubular pores that are continuously interwoven and branched to each other, forming a three-dimensional cubic phase (*Ia*3*d*) of the pores. This structure has also drawn the attention of researchers for their applicability in drug delivery[34–44] because the three-dimensional channel topography is attractive for developing systems designed to release drugs in an externally controlled manner.

Among molecular machines, a light-activated nanoimpeller utilizes the cis-trans photoisomerization of azobenzene derivatives.[45] When azobenzenes are immobilized to the silica pore walls and irradiated by a specific wavelength of light, which both cis and trans conformers absorb, a continuous photoisomerization of the azobenzene occurs.[46,47] This produces a constant wagging motion of the unbound terminus, driving the expulsion of loaded guest molecules from the pores.[18,19,48,49] In our laboratory, nanoimpellers have been utilized to externally control the release of molecules in solution[18–20,50] as well as deliver drug molecules in living cells.[18,50]

This chapter describes the synthesis and operation of a nanoimpeller-based release system built in the (*Ia*3*d*) cubic pore phase of the MCM-48 silica nanoparticles (Figure 4.1). The nanoparticles of MCM-48 were prepared at room temperature by modification of reported Stober procedures,[32,51] involving two additional synthetic strategies for particle functionalization. A co-condensation method was first used to derivatize the pores with a nanoimpeller during the synthesis.[19,47,52] External surfaces of the impeller-functionalized particles were then coated with

Rhodamine B-isothiocyanate (RITC) by a post-synthetic grafting strategy[19] for potential use of the material for intracellular imaging. After characterization of the particles, controlled release experiments were performed in solution by using the particles loaded with two categories of cargo molecules having different hydrophilicities such as water-soluble dyes (Propidium Iodide (PI), Rose Bengal, and 4',6-diamidino-2-phenylindole(DAPI)) and water-insoluble molecules (Camptothecin (CPT) and Rhodamine 6G (R6G)). Intracellular release of molecules was examined by *in vitro* cell studies on human cancer cells (a breast cancer cell line SK-BR3, and a pancreatic cancer cell line PANC-1) treated with the nanoimpeller-functionalized particles loaded with either PI dye or CPT drug.

4.3. Results and Discussion

4.3.1. Design and synthesis of MCM-48 nanoparticles functionalized with nanoimpellers

MCM-48 nanoparticles are synthesized by a base-catalyzed sol-gel process (similar to that of the more familiar MCM-41 synthesis) which involves micelle formation of surfactant, hydrolysis and condensation of an alkoxysilane, and removal of surfactant. Typically the surfactant cetyltrimethylammonium bromide (CTAB) is used to template the hexagonal pores of MCM-41 nanoparticles. The silica precursor tetraethylorthosilicate (TEOS) is added to the sol solution of CTAB and vigorously stirred for 2 h at 80 ºC. To obtain the cubic pores of MCM-48 nanoparticles, several different synthetic conditions are required such as higher surfactant concentration, lower (room) temperature, and the presence of a co-solvent (e.g. ethanol) according to reported procedures.[32,51] To optimize the surfactant concentration conditions and

obtain smaller and spherical particles, the synthesis of underivatized MCM-48 particles with a well-resolved cubic pattern of the pores was undertaken. The surfactant concentration was varied by changing the amount of the primary solvent, deionized water, while the synthesis temperature and the amount of the co-solvent ethanol were allowed to remain constant. After a series of trials, the cubic MCM-48 particles were synthesized using CTAB at a concentration that is about 4 times as high as that for the MCM-41 synthesis.[19] The cubic phase (*Ia3d*) of the unfunctionalized pores was confirmed by X-ray diffraction (XRD) (Figure 4.2). When the smaller surfactant dodecyltrimethylammonium bromide (DTAB) surfactant was used in attempts to make small pores, cubic structures were not obtained even when the concentration was increased by a factor of ~ 3.5.

Starting with the optimized surfactant concentration, incorporation of the derivatized azobenzene impellere into the silica framework was accomplished by a co-condensation strategy. This strategy consists of coupling the azobenzene with an organosilane linker in one container, followed by the addition of the coupled product to the CTAB surfactant solution in another flask for co-condensation with TEOS. For the coupling reaction, the azobenzene derivative 4-phenylazoaniline (4-PAA) and the organosilane linker isothiocyanatopropyltriethoxysilicate (ICPES) were chosen because the small size of the coupled azobenzene-linker (1.82 nm in length in the trans configuration) can fit into the CTAB-templated mesopore (ca. 2 nm in diameter).[47] Because the azobenzene moieties associate with the hydrophobic region of the CTAB micelles during the synthesis, the moving part of the azobenzene derivative is located in the hydrophobic region of the micelle that templates the pore pore while the alkoxysilane portion of the ICPES linkers are attached to the inner pore walls of the silica. After the surfactant molecules are

extracted after particle formation, the azobenzene end is free to undergo photoisomerization of the N=N bond inside the surfactant-free pore. In comparison to the synthesis of MCM-41-based nanoimpellers,[19] a factor of three lower molar ratio of 4-PAA/ TEOS was used for the synthesis of the azobenzene-functionalized MCM-48 nanoparticles. If the concentration of the azobenzene derivative that was added to the CTAB solution during the synthesis was the same as that used for the MCM-41 particles, hexagonally arranged pores were observed from the XRD pattern. By decreasing in the azobenzene concentration, the structural phase observed from the XRD pattern changes from the hexagonal to the cubic structure (Figure 4.3). This phase transformation is probably the result of the hydrophobic azobenzene molecules, which are positioned in the hydrophobic region of the CTAB micelles, disrupting the self-assembly of the micelles.

4.3.2. Physical morphologies of the nanoimpeller-derivatized MCM-48 nanoparticles

The surfactant-extracted particles were characterized by the X-ray diffraction pattern. Several characteristic peaks of the cubic *Ia3d* mesostructure were exhibited including a sharp first Bragg peak indexed as {211} at $2\theta = 2.51°$ and the second peak {220} at 2.89°. From the first peak, a lattice spacing of ~ 3.5 nm was calculated (Figure 4.4.A). Imaging by transmission and scanning electron microscopy shows that the particles have non-aggregated spherical shapes with an average size smaller than 500 nm, and reveals that the pore channels are three dimensionally linked and diverged (Figure 4.4.B). From the N_2 sorption isotherm of the particles (Figure 4.5), it was analyzed that the particles have a Brunauer–Emmett–Teller (BET) surface area of ~ 423 m^2g^{-1}, a total pore volume of ~ 0.23 cm^3g^{-1}, and an average pore diameter of ~ 2.3 nm.

The presence of the azobenzenes tethered into the cubic pores was confirmed by UV-Vis absorbance measurements of the particles suspended in methanol (Figure 4.6). From the absorption peak of the azobenzene at 366 nm, it was calculated that the particles contain about 3.4 wt% of the azobenzene machines and that about 2.4 azobenzene machines are attached on every 10 nm^2 of the silica framework in the pores.

4.3.3. Surface-labeling of the nanoimpeller-functionalized particles

The nanoimpeller-functionalized particles were further modified on the outer surfaces with a fluorescent molecule Rhodamine B isothiocyanate (RITC) in order to make the particle potentially suitable for *in vitro* intracellular imaging. Attachment of RITC molecules to the particles was performed by a post-synthetic grafting method derived from a previously reported strategy.[19] The linker aminopropyl-triethoxysilane (APS) was used to form a carbamide linkage to RITC. To complete the attachment, the nanoimpeller-assembled particles were mixed with APS in dry toluene overnight under N_2. The APS-modified particles were filtered and thoroughly washed with toluene, and then placed in an ethanolic solution of RITC and refluxed overnight under N_2. RITC-modified particles were recovered by filtration, washed thoroughly with ethanol, and then dried under vacuum. From UV-Vis spectroscopy of the particle suspension in methanol, the absorption peak of RITC was observed at 567 nm proving that RITC molecules are covalently bonded to the particles (Figure 4.6).

4.3.4. Photo-responsive operation of the nanoimpeller in the cubic mesopores

Light-activated operation of the nanoimpeller in the cubic pores was investigated by monitoring the fluorescence spectra of probe molecules. Several types of molecules having different hydrophilicities were chosen as cargo such as water-soluble dyes (Propidium Iodide (PI), Rose Bengal, and 4',6-diamidino-2-phenylindole (DAPI)) and water-insoluble hydrophobic molecules (Camptothecin (CPT) and Coumarine 540A (C540A)). For the spectroscopic measurements, the pores of the particles were loaded with the cargo molecules by soaking and stirring the particles in 1 mM solutions of the cargo for ~ 24 h at room temperature in the light, followed by washing and drying under vacuum in the dark. Cargo-loaded particles were then placed in a corner of the cuvette, which was carefully filled with the chosen liquid without disturbing the particles. A probe beam was directed to the liquid above the particles to detect dissolved cargo molecules that are released from the particles. An excitation beam was then turned on to irradiate the cargo-loaded particles and activate the azobenzene motion as shown in the Figure 4.7. The wavelength of the excitation beam was 413 nm, a wavelength where both trans and cis isomers of the derivatized azobenzene have about the same extinction coefficients.[46] The wavelength of the probe beam was chosen to match the absorption spectrum of the cargo molecules and thus optimize the fluorescence intensity. To obtain a release profile of the cargo, the fluorescence spectra of the molecules released into solution were continuously measured, and the intensity at the emission peak maximum were plotted as a function of time at 1 second intervals.

4.3.4.1. Release of hydrophilic cargo molecules

The stimulated release was first tested in aqueous solution by using the azobenzene-

derivatized particles loaded with the water-soluble dyes PI, Rose Bengal, and DAPI. For the particles loaded with PI (M.W. ~ 668 g/mol), a probe beam wavelength of 514 and a 413 nm excitation beam wavelength were used. The release profile of PI is shown in Figure 4.8.A. The initial flat baseline for ~5 min shows that the loaded PI molecules were held in the cubic pores without leakage prior to the light stimulation. When the pump laser beam was turned on to activate the azobenzene, an increase in the fluorescence intensity was observed, indicating that the dyes were released from the particles. The weight percentage of the released PI molecules from the particles, measured after one hour by UV-Vis spectroscopy, was 1.2 wt%.

Particles were also loaded with another hydrophilic dye Rose Bengal (M.W. ~ 1,017 g/mol), which has a larger molecular size, and were tested for the photo-stimulatedd release using the same spectroscopic procedure as described above. A similar pattern of the release profile ($\lambda \approx 575$ nm) was observed. There was minimal leakage from the particles in the dark and when stimulated with 413 nm light, the particles released Rose Bengal molecules from the cubic pores increasing the fluorescence intensities (Figure 4.9).

The final water-soluble dye that was tested, DAPI (M.W. ~ 350 g/mol), was loaded into the particles functionalized with both azobenzene and RITC. For the real time measurement of the DAPI release from the particles, 413 nm was used as a both probe and pump beam. Fluorescence intensities ($\lambda \approx 500$ nm) remained about the same for the initial 10 min before the DAPI-loaded particles were illuminated by 413 nm beam. Upon stimulation of the particles the emission intensity from the released DAPI rose similar to that of the other dyes (Figure 4.8.B). These results from the different water-soluble dyes clearly show that the nanoimpellers attached to the pores of the cubic-phase nanoparticles can be successfully operated in aqueous solution. In

addition, the DAPI release from the RITC-modified particles demonstrates that the presence of the RITC molecules attached to the external surfaces does not inhibit the escape of RITC molecules through the pore orifices.

4.3.4.2. Release in a non-aqueous environment of water-insoluble probe molecules

Nanoimpellers of the type described in this paper have an advantage over many of the cap-and-release systems that have been studied: they can operate in non-aqueous solutions. For example, reversible caps such as those based on cyclodextrin[17,24,53–55] or cucubit[6]uril[26] that rely on hydrophobic-hydrophobic interaction for binding and activation can only be operated in water. Because the nano-impellers rely on the photo-stimulated large amplitude motion of the azobenzene unit and can be operated in a wide variety of non-aqueous media, they offer an extended versatility.

The release experiments using camptothecin (CPT) as the cargo molecule in a non-aqueous environment were carried out in dimethyl sulfoxide (DMSO). CPT is a well-known fluorescent anticancer drug, and it has been demonstrated that a MCM-41-based nanoimpeller can deliver and release CPT into human cancer cells and cause apoptosis under photocontrol.[18,56] The cubic-phase particles functionalized with both impellers and RITC were loaded with CPT in DMSO. The cuvette containing the CPT-loaded particles was also filled with DMSO for the spectroscopic release studies. As shown in Figure 4.10, the un-activated static machine in the dark clogged the cubic pores and kept the CPT molecules from escaping the pores. Upon photoexcitation the dynamic back-and-forth wagging motion of the activated nanoimpeller drove the expulsion of CPT from the pores into the DMSO. It was calculated from the UV-Vis

absorption spectra ($\lambda \sim 366$ nm) that the amount of CPT released into DMSO was ~ 0.25 wt% of the impeller-functionalized particles after ~ 1 h irradiation of the particles.

Operation of the nanoimpeller in methanol was also demonstrated by using the laser dye C540A. Azobenzene-assembled particles were loaded with the dye in methanol. The wavelength of 457 nm was chosen to probe released molecules and also to excite the azobenzene. Because the azobenzene has a lower extinction coefficient at 457 nm,[46] this wavelength is not optimal to excite the wagging motion and thus causes a lower release efficiency of the particles. Nevertheless, photo-responsive release behavior of the particles was observed with minimal leakage (Figure 4.11), again demonstrating that the azobenzene impeller attached inside the silica pore is stable in both hydrophilic and hydrophobic solution and photoisomerization of the azobenzene is constantly reproduced under external control.

4.3.5. Intracellular release of drugs

Based on the successful release of various molecules in different solutions, MCM-48-supported nanoimpellers were tested for biological applicability by *in vitro* cell studies on a human breast cancer cell line (SK-BR3) and a human pancreatic call line (PANC-1) using two different cargo molecules - PI (membrane-impermeable cell staining dye), and CPT (anti-cancer drug), respectively. For the intracellular release of PI, SK-BR3 cells were treated with a suspension of the azobenzene-derivatized particles loaded with PI (10 or 20 μg/ml). After 3 h incubation, the cells were washed with PBS buffer to remove the particles that were not taken up by the cells. The cells containing the PI-loaded particles were either left in the dark or irradiated for 5 min with 413 nm light (~ 0.13 W/cm^2), and then examined by confocal microscopy 30 min

later. Minimal staining of the nuclei was observed in the cells that were kept in the dark (Figure 4.12.A). When the impellers were excited, PI molecules were released from the particles and stained the cell nuclei red (Figures 4.12.B-C). When another cell line, PANC-1, was loaded with RITC-labeled particles containing CPT (100 μg/ml), cell apoptosis was induced under photo-control. Without light stimuli, the CPT remained inside the cubic pores and it did not cause cell death. Illumination, however, expelled the CPT molecules from the particles, which induced nuclear fragmentation and cell death (Figure 4.12.D).

4.4. Summary

The nanoimpeller system can be installed in cubic-structured mesoporous silica nanoparticles and operated under photocontrol. Underivatized silica surfaces, containing hydrophilic silanol groups, were functionalized to include chemically bonded hydrophobic azobenzenes, which possibly helped load both hydrophobic and hydrophilic cargos in the pores respectively via corresponding molecular interactions. Release experiments of molecules were accomplished in aqueous, non-aqueous and intracellular environments using a variety of cargo molecules. The operation of the azobenzene impeller can be photocontrolled both in hydrophilic and hydrophobic solutions. The complex cubic structure of the pores that are curved and branched three dimensionally with a very high surface area potentially offers the possibility of increasing the loading. Further studies are in progress for biomedical applications of the cubic phase nanoparticles as a functional silica nanocontainer with a higher surface area and an increased drug loading efficiency.

4.5. Experimental

4.5.1. Characterization

Powder X-ray diffraction measurements were carried out using a Panalytical X'Pert Pro powder diffractometer equipped with copper radiation ($K\alpha_1$ and $K\alpha_2$ = 1.5418 Å). Transmission electron microscope (TEM) image was collected on a JEM1200-EX (JEOL) instrument in the California NanoSystem Institute (CNSI). Scanning electron microscope (SEM) images were obatined on a JEOL SM-71010 instrument. Au coating of the particles used for imaging was carried out by sputtering for 1 min (Hummer 6.2, Anatech LTD, plasma discharge current = 15 mA at 70 mTorr). UV-Vis spectra were collected using a Cary 5000 UV-Vis-NIR spectrophotometer. The controlled release profiles were obtained via luminescence spectroscopy using an Acton SpectraPro 2300i CCD and a coherent Krypton Innova 300C and Argon Innova 90C-5-excitation laser. Nitrogen adsorption-desorption isotherm was obtained at 77 K on a Quantachrome Instruments NOVA 4200e. The specific surface area was calculated using the Brunauer-Emmet-Teller (BET) model. Pore size and pore volume were determined from the adsorption data by the Barrett-Joyner- Halenda (BJH) method.

4.5.2. Preparation of nanoimpeller-functionalized MCM-48 nanoparticles

All of the chemicals for the particle synthesis were purchased from Sigma-Aldrich. 17.3 mg of the small azobenzene derivative 4-phenylazoaniline (4-PAA) was first reacted with 87 μL of the organosilane linker isothiocyanatopropyltriethoxysilicate (ICPES) by refluxing them in 1mL ethanol under N_2 for ~ 4 h.[47,52] During the coupling reaction, a surfactant solution was prepared in another flask by stirring 1.2 g of cetyltrimethylammonium bromide (CTAB), 6.86

mL of NH_4OH, 25 mL of EtOH, and 50 mL of the deionized H_2O for 30 min at room temperature. To this solution, 1.82 mL of tetraethylortho silicate (TEOS) and the coupled 4-PAA-ICPES were slowly added and stirred vigorously for 2 h at room temperature. The synthesized particles were recovered by filtration with washing with methanol. To remove the surfactant, suspension of the as-prepared particles was refluxed in a mixture of HCl and methanol for ~ 12 h.

4.5.3. RITC-modification of the azobenzene-derivatized particles

Aminopropyltriethoxysilicate (APS) was first attached to the outer surfaces of the particles by suspending 0.1 g of the surfactant-removed azobenzene-derivatized particles in 10 mL of dry toluene with 23.4 μL of APS and refluxing overnight under N_2. After filtration and washing with toluene, the APS-modified particles were mixed with 13.4 mg of Rhodamine B isothiocyanate (RITC) dissolved in 5 mL of ethanol. This particles suspension was refluxed overnight under N_2, after which the particles were filtered, thoroughly washed with ethanol, and dried under vacuum.

4.5.4. Cargo loading procedure

To load cargo molecules in the pores, ~ 20 mg of the particles were soaked and stirred in appropriate solution of the cargo (1 mM) for ~ 24 h at room temperature in the normal light (deionized water for propidium iodide (PI), Rose Bengal, and 4', 6-diamidino-2-phenylindole (DAPI); dimethyl sulfoxide (DMSO) for camptothecin (CPT); MeOH for Coumarin 540A (C540A)). These particle suspensions were then centrifuged and the supernatant solution was removed. The particles were re-suspended in a fresh solution and centrifuged again. This

procedure was repeated at least twice until the supernatant solution after the centrifuge appeared clear. Cargo-loaded particles were then dried under vacuum.

4.5.5. Controlled release experiment

Particles loaded with cargo molecules were carefully placed in a corner of a cuvette, which was filled with one of deionized water, DMSO, and MeOH. The probe beam (20 mW, 514 nm for PI and Rose Bengal; 5 mW, 413 nm for DAPI; 3 mW, 413 nm for CPT; 1 mW, 457 nm for C540A) was directed into the liquid above the particles to excite fluorescent released cargo molecules. Then a pump beam was directed at the particles and turned on to activate the azobenzene motion (20 mW, 413 nm for PI and Rose Bengal; 45 mW, 413 nm for DAPI; 27 mW, 413 nm for CPT; 9 mW, 457 nm for C540A). The release profiles were obtained by plotting the fluorescence intensities at the emission maximum as a function of time.

4.5.6. UV-Vis absorbance measurement of the released amount of molecules

To determine the released amount of PI from the nanoimpeller-functionalized particles, 10 mg of the particles loaded with PI were suspended and sonicated with 4 mL of deionized water, placed in a cuvette, and irradiated by ~ 0.2 W/cm^2, 413 nm light for 1h. The particle suspension was then centrifuged and the UV-Vis absorption spectrum of the supernatant solution containing the released PI molecules was measured. The same procedure was repeated for the CPT-loaded particles except that the particles were treated with DMSO and irradiated by ~ 0.15 W/cm^2, 413 nm light.

4.5.7. Confocal fluorescence imaging of cells

Human breast cancer cells (SK-BR3) were obtained from the American-type culture collection and were maintained in Dulbec-co's modified Eagle's medium (DMEM) (GIBCO)

and Leibovitz's L-15 medium (Cellgro), respectively, supplemented with 10 % fetal calf serum (Sigma, MO), 2 % L-glutamine, 1 % penicillin, and 1 % streptomycin stock solutions with regular passage. 4000 cells were seeded in Lab-Tek chamber slide system for overnight before treated with 10 or 20 μg/ml PI-loaded nanoimpeller-functionalized MCM-48 particles for 3 hours. The SK-BR3 cells with PI-loaded particles were then either left in the dark or irradiated by ~ 0. 13 W/cm^2, 413 nm light for 5 min, and examined with fluorescence microscopy.

4.6. Figures

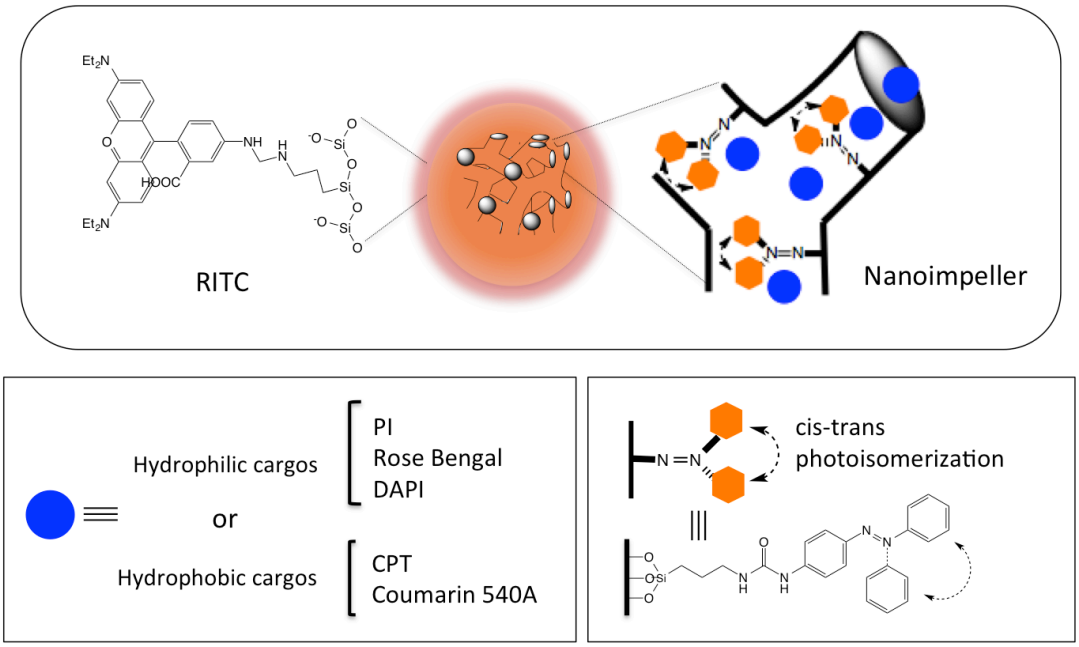

Figure 4.1. Schematic depiction of mechanized MCM-48 nanoparticles for photocontrolled release of molecules. Particles have the pore channels that are three dimensionally interconnected in the cubic phase (*Ia*3*d*). The interiors of the pores (~2.3 nm in diameter) are functionalized with azobenzene derivatives by the co-condensation method, and the external surfaces of the particles are modified with RITC by post-synthetic grafting. The pores are loaded with either hydrophilic or hydrophobic molecules to test the operation of the azobenzene nanoimpeller. Continuous illumination at 413 nm (or 457 nm) causes a constant cis-trans photoisomerization of the azobenzene producing dynamic wagging motion of the untethered terminus and releases the molecules from the pores.

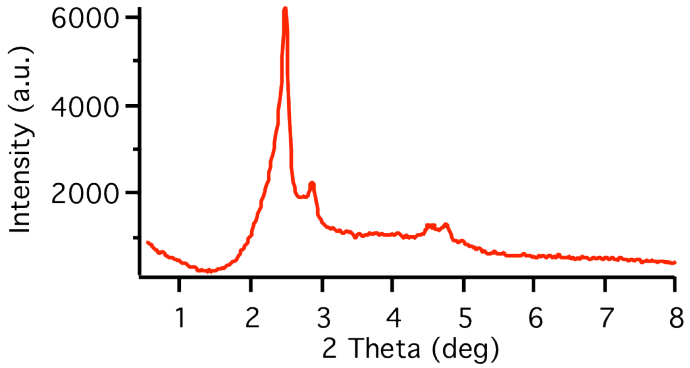

Figure 4.2. XRD pattern of underivatized MCM-48 nanoparticles. The typical peaks of the MCM-48 silica were exhibited indicating the well-ordered cubic structure of the pores.

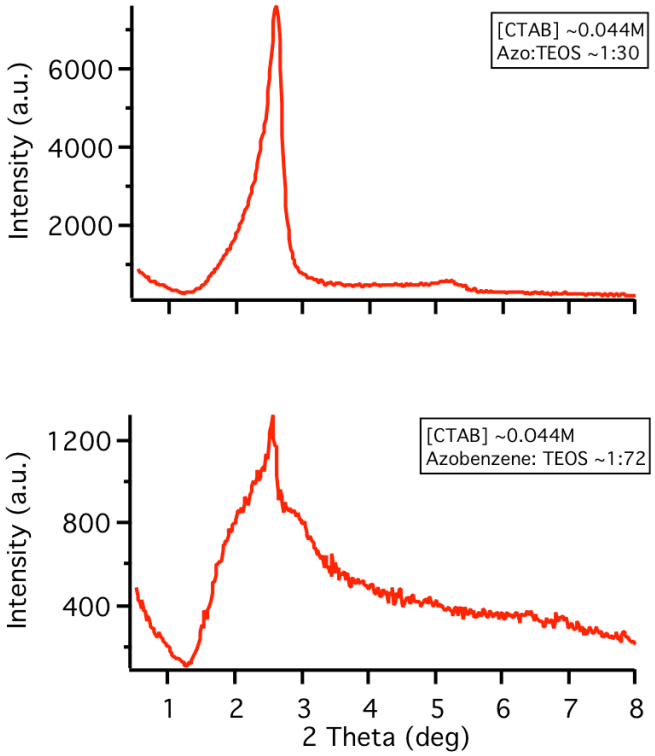

Figure 4.3. XRD pattern of the nanoimpeller-functionalized MCM-48 particles synthesized by using a different molar ratio of azobenzenze/ TEOS. When a higher amount of the azobenzene was used for the synthesis (4-PAA: TEOS = ~ 1:30), the MCM-41-type diffraction pattern was exhibited, indicating the formation of hexagonal pores (A). With decrease in the amount of the azobenzene (4-PAA: TEOS = ~ 1:72), the hexagonal-to-cubic phase transition of the pores was indicated (B).

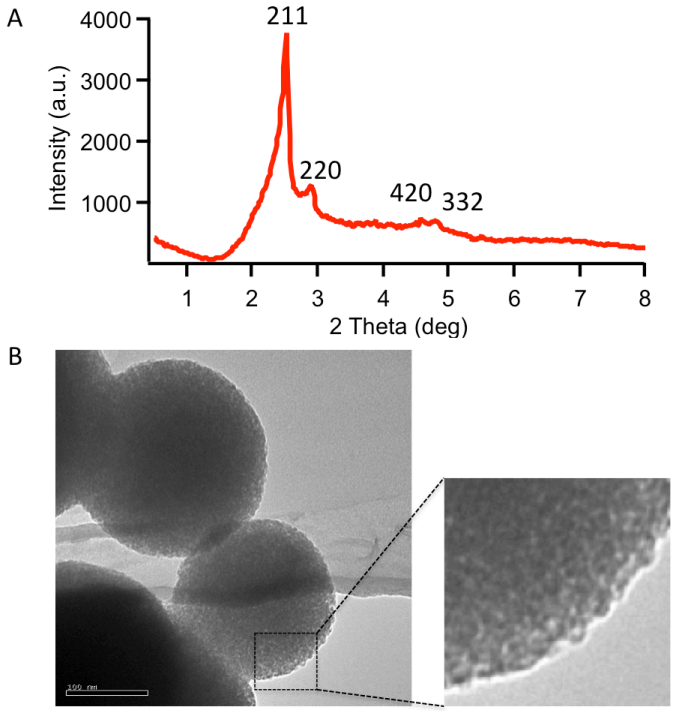

Figure 4.4. Characterization of the nanoimpeller-derivatized MCM-48 nanoparticles after surfactant removal. A) X-ray diffraction (XRD) pattern and B) transmission electron microscopy (TEM) image of the particles. The XRD of the particles exhibits well-resolved characteristic peaks of the cubic mesopores of MCM-48 silica, including the first peak indexed as (211) at 2θ = 2.51° and the second peak (220) at 2.89°. The magnified portion of the TEM image reveals the pores that are branched and interconnected.

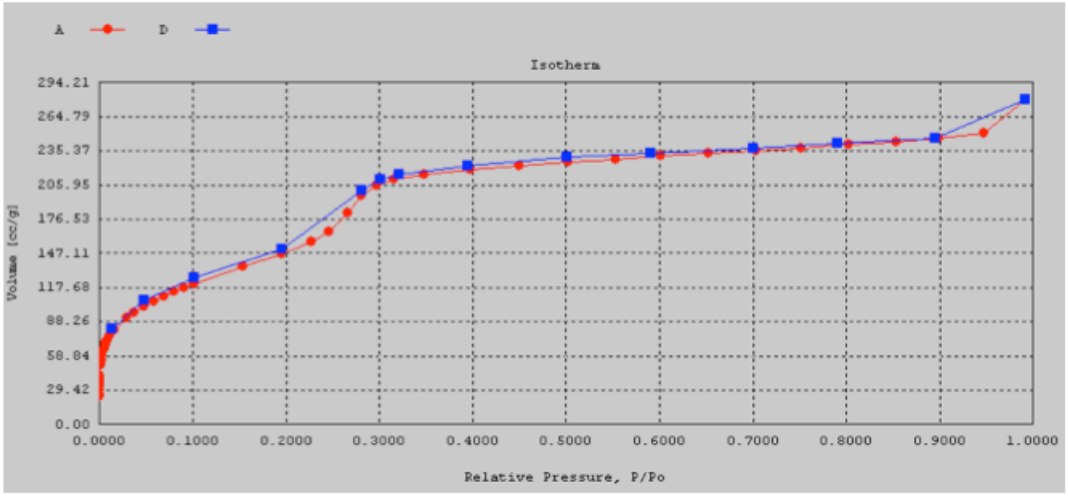

Figure 4.5. Nitrogen adsorption-desorption isotherm of the unfunctionalized MCM- 48 nanoparticles after the surfactant is removed from the pores. Increase of the volume between 0.2 and 0.3 indicates the capillary condensation of the nitrogen gas at the internal mesopores, confirming the type IV isotherm that is typically observed for mesoporous nanoparticles.

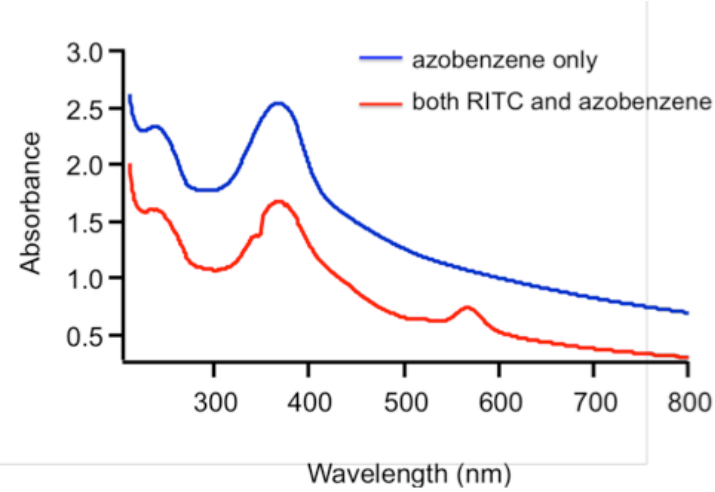

Figure 4.6. UV-Vis absorbtion spectra of a methanolic suspension of particles functionalized with only nanoimpeller (blue) and both impeller and RITC (red). From the absorption peaks, it was confirmed that the particles were successfully functionalized with the azobenzene ($\lambda \sim 366$ nm) and the RITC molecules ($\lambda \sim 567$ nm).

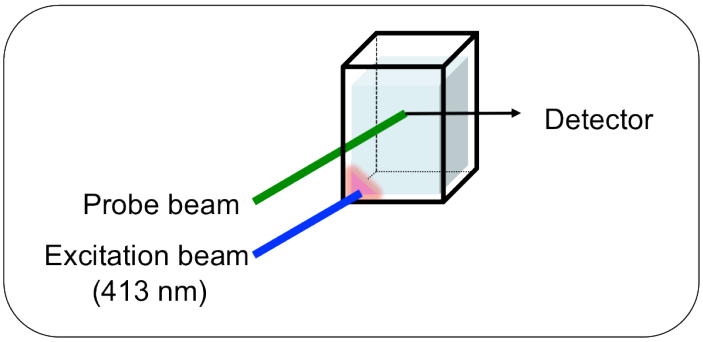

Figure 4.7. Spectroscopic measurements for the controlled release measurement. The probe beam is directed to the liquid above the particles to excite the dye molecules released from the particles. The pump beam (413 or 457 nm) is directed at the particles and turned on to activate the azobenzenes' motions. Fluorescence intensities of the dye molecules released from the particles are monitored by a monochromator and CCD detector as a function of time.

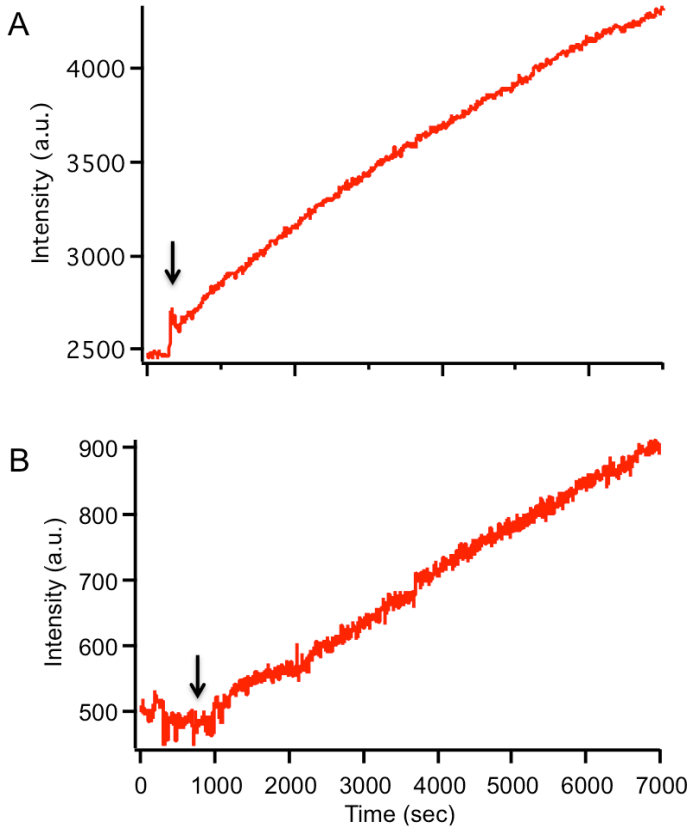

Figure 4.8. Release of hydrophilic cargo molecules PI (A) and DAPI (B) into water from the nanoimpeller-functionalized MCM-48 nanoparticles. No or negligible release of the dyes was observed in the dark, as shown by the flat baseline of the emission intensities. The intensities increased as the dyes were released from the particles after the pump beam (413 nm) was turned on to activate the azobenzene machine at the times indicated by the arrows.

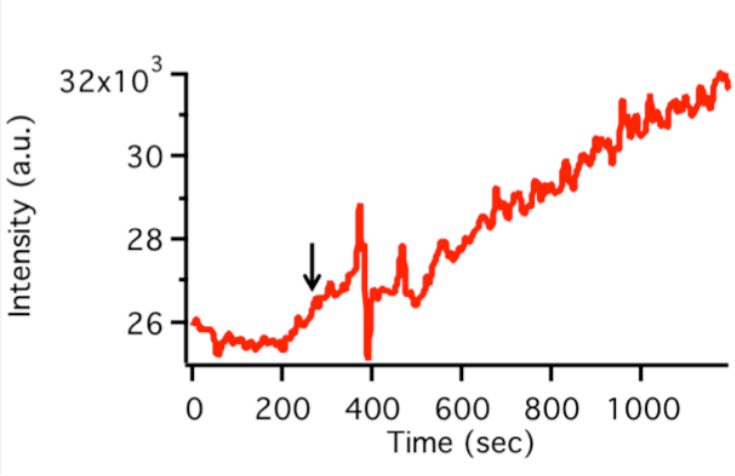

Figure 4.9. Release of Rose Bengal dye into water from the nanoimpeller- functionalized particles. There was slight leakage in the dark. Upon excitation by 413 nm light at 300 sec., the particles released Rose Bengal molecules from the cubic pores and the emission intensities increased.

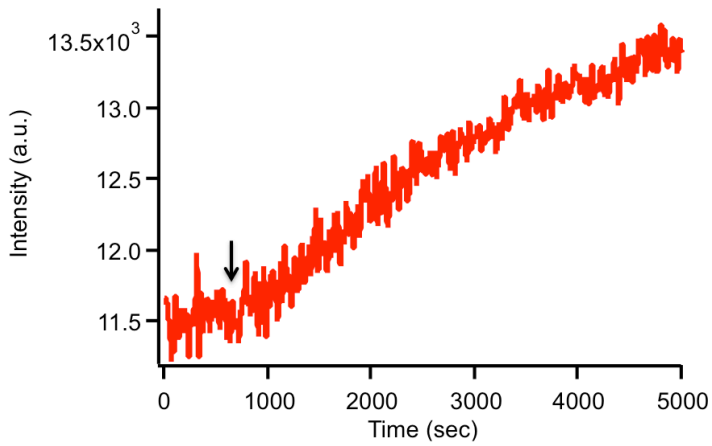

Figure 4.10. Release of a hydrophobic drug CPT into DMSO from the MCM-48 nanoparticles functionalized with both nanoimpellers and RITC. The arrow indicates the time when the azobenzene activation light (413 nm) was turned on. There is negligible leakage in the dark, and CPT is released from the cubic pores in response to the light stimulation, increasing the fluorescence intensities.

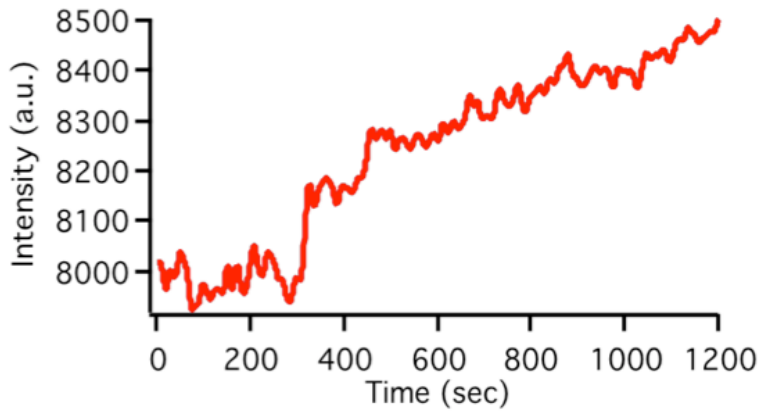

Figure 4.11. Release of C540A dye into methanol from the nanoimpeller- functionalized particles. A longer wavelength of light, 457 nm was used to activate the azobenzene and was turned on at 300 sec.

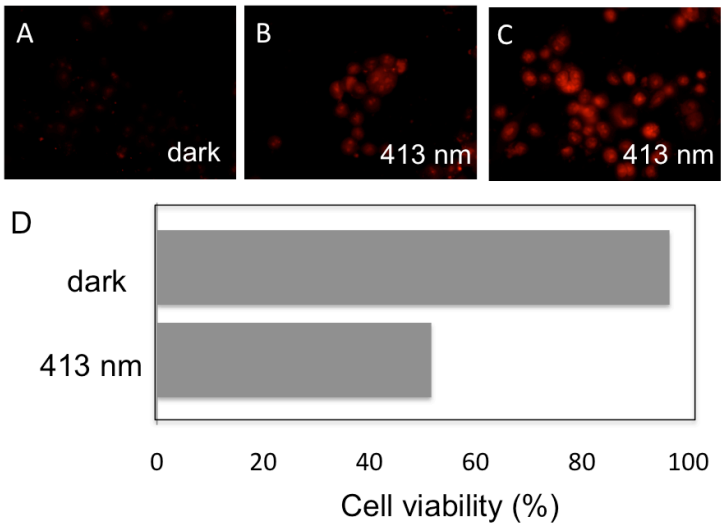

Figure 4.12. Intracellular release of PI and CPT. A-C: confocal fluorescence images of SK-BR3 cancer cells that were treated with a suspension of 10 μg/ml (B) or 20 μg/ml (A, C) particles loaded with PI, left in the dark (A), and illuminated for 5 minutes with 413 nm light (B-C). Photoactivated impellers released PI molecules from the particles, staining the cell nuclei red (B-C), but unexcited machines caused no staining of the nuclei (A). D: *in vitro* cytotoxicity assay of PANC-1 cancer cells that were treated with a suspension of 100 μg/ml particles loaded with CPT, left in the dark, and illuminated for 5 minutes with 413 nm light. Cell apoptosis was caused by CPT molecules expelled from the light-activated nanoimpeller-functionalized particles. The cell viability was determined by using the cell counting kit.[18]

4.7. References

[1] J. S. B. C.T. Kresge, M.E. Leonowicz, W.J. Roth, J.C. Vartuli, *Nature* **1992**, *359*, 710–712.

[2] J. S. Beck, K. D. Schmitt, J. B. Higgins, J. L. Schlenkert, *J. Am. Chem. Soc.* **1992**, *114*, 10834–10843.

[3] M. W. Ambrogio, C. R. Thomas, Y.-L. Zhao, J. I. Zink, J. F. Stoddart, *Acc. Chem. Res.* **2011**, *44*, 903–13.

[4] I. I. Slowing, B. G. Trewyn, S. Giri, V. S.-Y. Lin, *Adv. Funct. Mater.* **2007**, *17*, 1225–1236.

[5] J. Vallet-Regi, M., Ramila, A., Del Real, R. P., Perez-Pariente, *Chem. Mater.* **2001**, *13*, 308–311.

[6] I. I. Slowing, J. L. Vivero-Escoto, C.-W. Wu, V. S.-Y. Lin, *Adv. Drug Deliv. Rev.* **2008**, *60*, 1278–88.

[7] S. Angelos, E. Johansson, J. F. Stoddart, J. I. Zink, *Adv. Funct. Mater.* **2007**, *17*, 2261–2271.

[8] K. K. Cotí, M. E. Belowich, M. Liong, M. W. Ambrogio, Y. A. Lau, H. A. Khatib, J. I. Zink, N. M. Khashab, J. F. Stoddart, *Nanoscale* **2009**, *1*, 16–39.

[9] D. Tarn, C. E. Ashley, M. I. N. Xue, E. C. Carnes, J. I. Zink, C. J. Brinker, *Acc. Chem. Res.* **2013**, *46*, 792–801.

[10] Z. Li, J. C. Barnes, A. Bosoy, J. F. Stoddart, J. I. Zink, *Chem. Soc. Rev.* **2012**, *41*, 2590–605.

[11] R. Ballardini, V. Balzani, A. Credi, M. T. Gandolfi, M. Venturi, *Acc. Chem. Res.* **2001**, *34*, 445–455.

[12] V. Balzani, Ä. Pez, J. F. Stoddart, **1998**, *31*, 405–414.

[13] W. R. Browne, B. L. Feringa, *Nat. Nanotechnol.* **2006**, *1*, 25–35.

[14] L. Mu, S. S. Feng, *J. Control. Release* **2003**, *86*, 33–48.

[15] S. Febvay, D. M. Marini, A. M. Belcher, D. E. Clapham, *Nano Lett.* **2010**, *10*, 2211–9.

[16] R. Huschka, O. Neumann, A. Barhoumi, N. J. Halas, *Nano Lett*. **2010**, *10*, 4117–22.

[17] D. P. Ferris, Y.-L. Zhao, N. M. Khashab, H. A. Khatib, J. F. Stoddart, J. I. Zink, *J. Am. Chem. Soc*. **2009**, *131*, 1686–8.

[18] J. Lu, E. Choi, F. Tamanoi, J. I. Zink, *Small* **2008**, *4*, 421–426.

[19] S. Angelos, E. Choi, F. Vo, L. De Cola, J. I. Zink, *J. Phys. Chem. C* **2007**, *111*, 6589–6592.

[20] S. Saha, L.E. Johansson, A.H. Flood, H.-R. Tseng, J.I. Zink and J.F. Stoddart , *Chem. Eur. J*. **2005**, 11, 6846-6858

[21] N. K. Mal, M. Fujiwara, Y. Tanaka, T. Taguchi, M. Matsukata, *Chem. Mater*. **2013**, *15*, 3385–3394.

[22] S. Angelos, M. Liong, E. Choi, J. I. Zink, *Chem. Eng. J*. **2008**, *137*, 4–13.

[23] D. Tarn, M. Xue, J. I. Zink, *Inorg. Chem*. **2013**, *52*, 2044–9.

[24] Y.-L. Zhao, Z. Li, S. Kabehie, Y. Y. Botros, J. F. Stoddart, J. I. Zink, *J. Am. Chem. Soc*. **2010**, *132*, 13016–25.

[25] M. Xue, D. Cao, J. F. Stoddart, J. I. Zink, *Nanoscale* **2012**, *4*, 7569–74.

[26] S. Angelos, N. M. Khashab, Y.-W. Yang, A. Trabolsi, H. A. Khatib, J. F. Stoddart, J. I. Zink, *J. Am. Chem. Soc*. **2009**, *131*, 12912–4.

[27] K. C. Leung, T. D. Nguyen, J. F. Stoddart, J. I. Zink, *Chem. Mater*. **2006**, *18*, 5919–5928.

[28] T. D. Nguyen, H.-R. Tseng, P. C. Celestre, A. H. Flood, Y. Liu, J. F. Stoddart, J. I. Zink, *Proc. Natl. Acad. Sci. U. S. A*. **2005**, *102*, 10029–34.

[29] C. R. Thomas, D. P. Ferris, J.-H. Lee, E. Choi, M. H. Cho, E. S. Kim, J. F. Stoddart, J.-S. Shin, J. Cheon, J. I. Zink, *J. Am. Chem. Soc*. **2010**, *132*, 10623–5.

[30] J. Kim, H. S. Kim, N. Lee, T. Kim, H. Kim, T. Yu, I. C. Song, W. K. Moon, T. Hyeon, *Angew. Chem. Int. Ed. Engl*. **2008**, *47*, 8438–41.

[31] J. Croissant, J. I. Zink, *J. Am. Chem. Soc*. **2012**, *134*, 7628–31.

[32] B. K. Schumacher, F. Von Hohenesche, K. K. Unger, R. Ulrich, A. Du Chesne, U. Wiesner, H. W. Spiess, *Adv. Mater*. **1999**, *11*, 1194–1198.

[33] K. Schumacher, P. I. Ravikovitch, A. Du Chesne, A. V. Neimark, K. K. Unger, *Langmuir* **2000**, *16*, 4648–4654.

[34] M. Vallet-Regí, F. Balas, D. Arcos, *Angew. Chem. Int. Ed. Engl.* **2007**, *46*, 7548–58.

[35] I. Izquierdo-Barba, E. Sousa, J. C. Doadrio, A. L. Doadrio, J. P. Pariente, A. Martínez, F. Babonneau, M. Vallet-Regí, *J. Sol-Gel Sci. Technol.* **2009**, *50*, 421–429.

[36] I. Izquierdo-Barba, A. Martinez, A. L. Doadrio, J. Pérez-Pariente, M. Vallet-Regí, *Eur. J. Pharm. Sci.* **2005**, *26*, 365–73.

[37] F. Qu, G. Zhu, H. Lin, W. Zhang, J. Sun, S. Li, S. Qiu, *J. Solid State Chem.* **2006**, *179*, 2027–2035.

[38] M. Fernández-Núñez, D. Zorrilla, A. Montes, M. J. Mosquera, *J. Phys. Chem. A* **2009**, *113*, 11367–75.

[39] Y.-F. Zhu, J.-L. Shi, Y.-S. Li, H.-R. Chen, W.-H. Shen, X.-P. Dong, *J. Mater. Res.* **2011**, *20*, 54–61.

[40] P. Yang, P. Yang, X. Teng, J. Lin, L. Huang, *J. Mater. Chem.* **2011**, *21*, 5505.

[41] M. Vafaee, M. M. Amini, E. Najafi, O. Sadeghi, V. Amani, *J. Sol-Gel Sci. Technol.* **2012**, *64*, 411–417.

[42] A. Popat, J. Liu, Q. Hu, M. Kennedy, B. Peters, G. Q. M. Lu, S. Z. Qiao, *Nanoscale* **2012**, *4*, 970–5.

[43] S. Gai, P. Yang, D. Wang, C. Li, N. Niu, F. He, M. Zhang, J. Lin, *RSC Adv.* **2012**, *2*, 3281.

[44] A. Liu, S. Han, H. Che, L. Hua, *Langmuir* **2010**, *26*, 3555–61.

[45] G. S. Hartley, *Nature* **1937**, 281.

[46] P. Sierocki, H. Maas, P. Dragut, G. Richardt, F. Vögtle, L. De Cola, F. a M. Brouwer, J. I. Zink, *J. Phys. Chem. B* **2006**, *110*, 24390–8.

[47] N. Liu, Z. Chen, D. R. Dunphy, Y.-B. Jiang, R. A. Assink, C. J. Brinker, *Angew. Chem Int. Ed.* **2003**, *42*, 1731–4.

[48] Y. Zhu, M. Fujiwara, *Angew. Chem. Int. Ed. Engl.* **2007**, *46*, 2241–4.

[49] N. Liu, D. R. Dunphy, P. Atanassov, S. D. Bunge, Z. Chen, G. P. Lo, T. J. Boyle, C. J. Brinker, *Nano Lett*. **2004**, *4*, 551–554.

[50] Y. A. Lau, B. L. Henderson, J. Lu, D. P. Ferris, F. Tamanoi, J. I. Zink, *Nanoscale* **2012**, *4*, 3482–9.

[51] T.-W. Kim, P.-W. Chung, V. S.-Y. Lin, *Chem. Mater*. **2010**, *22*, 5093–5104.

[52] S. Huh, J. W. Wiench, J. Yoo, M. Pruski, V. S. Lin, *Chem. Mater*. **2003**, *15*, 4247–4256.

[53] H. Meng, M. Xue, T. Xia, Y.-L. Zhao, F. Tamanoi, J. F. Stoddart, J. I. Zink, A. E. Nel, *J. Am. Chem. Soc*. **2010**, *132*, 12690–7.

[54] K. Patel, S. Angelos, W. R. Dichtel, A. Coskun, Y.-W. Yang, J. I. Zink, J. F. Stoddart, *J. Am. Chem. Soc*. **2008**, *130*, 2382–3.

[55] L. Du, S. Liao, H. A. Khatib, J. F. Stoddart, J. I. Zink, *J. Am. Chem. Soc*. **2009**, *131*, 15136–42.

[56] J. Lu, M. Liong, J. I. Zink, F. Tamanoi, *Small* **2007**, *3*, 1341–6.

CHAPTER 5.

Bifunctional Mesoporous Silica Nanoparticles for

Simultaneous Cancer Therapy

5.1. Abstract

In this chapter, a simultaneous cancer therapy system is installed on a single particle of mesoporous silica combining the photodynamic therapy (PDT) using a photosensitizer and the chemotherapy using an anticancer drug. MSNs are first synthesized with the pores functionalized with a photosensitizer porphyrin (PP) derivative that is able to produce cytotoxic singlet oxygen molecules. Next, an anticancer drug camptothecin (CPT), which is able to induce programmed cell death called apoptosis, is loaded in the mesopore of the PP-functionalized MSN. Singlet oxygen generation was confirmed by its infrared luminescence spectra and the photo-oxidation of a singlet oxygen trapping agent, 1,3-diphenylisobenzofuran (DPBF). *In vitro* studies on a human pancreatic cancer cell line (PANC-1) demonstrate that a synergetic cancer treatment can be achieved when this MSN is taken up by cells and illuminated with 647 nm light, caused by both the CPT release and the singlet oxygen generated from the photoexcited PP derivative.

5.2. Introduction

Among various cancer treatment methods, chemotherapy using anticancer drug is one of the most popular treatments. One of the potent anticancer drugs, camptothecin (CPT) has a high efficiency to induce a programmed cell death via apoptosis, which has been demonstrated in several cell studies.[1–5] However, clinical applications of CPT have been limited due to its poor solubility in aqueous media. Synthesis researchers have succeeded in enhancing its water solubility by modifying its chemical structure at a cost of reducing its anticancer treatment efficiency.[6–8]

An alternative type of the cancer therapy, photodynamic therapy (PDT), is a system that utilizes photosensitizers that produce cytotoxic reactive oxygen species (ROS) such as singlet oxygen and free radicals when irradiated with specific wavelengths of light.[9] Photo-responsivity of the PDT system has several attractive features. Above all, ease in turning light on and off enables the system to be controlled at a distance and at a specific time on demand. Also, facile control to focus light radiation only on the area of interest prevents the surrounding tissue from the harmful ROS. Porphyrin photosensitizing agents have been widely reviewed because of the high effectiveness for singlet oxygen generation.[9–17] Protoporphyrin (PP) is especially clinically promising because it has light absorption at longer wavelengths of visible light (up to ~ 650 nm), which allows for deeper tissue penetration. Similar to CPT, however, its hydrophobicity has been problematic.[18]

Mesoporous silica nanoparticles (MSNs) synthesized by sol-gel chemistry[19–21] have been intensely studied in the recent biomedical research because of the biocompatibility and multifunctionality. The uniform mesopores with a large surface area (> 1,000 m^2/g) have been extensively utilized as molecular containers for various drug loading. Also, MSNs can be functionalized with a wide range of biologically useful organic molecules or inorganic nanocrystals. Examples of the functionalities include controlled drug release,[22–28] cell targeting and imaging,[29] and antibacterial activities.[30] With recent development of various synthetic techniques, physical morphologies of the particles (i.e. shape and size of the pores and the particles) have been optimized for biomedical applications, and tested *in vitro* and *in vivo*.[31,32]

In this chapter, MSN is functionalized such that two different cancer therapies are combined on a single particle: (1) a chemotherapy using a an anticancer drug CPT that is stored

in and released out of the mesopores[22,23,33] and (2) the PDT using a photosensitizer PP derivative that is chemically bonded to the pore wall and allowed to generate singlet oxygen by light irradiation[34] (Figure 5.1). Human pancreatic cancer cells (PANC-1) were exposed to suspensions of the particles for the endocytosis process, and illuminated with 647 nm light to excite PP. Quantatative cell survival assay indicates that singlet oxygen produced by the photoexcited PP results in cell death, depending on the dosage and the light illumination time. When the particles loaded with CPT were treated with cells and light, cell death was increased to a larger degree, indicating that CPT and singlet oxygen simultaneously caused toxicities to the cells.

5.3. Results and Discussion

5.3.1 Synthesis and Characterization of the Porphyrin-modified MSNs

The MSN functionalized with a porphyrin photosensitizer was synthesized by a base-catalyzed sol-gel process involving a co-condensation method[35], using cetyltrimethylammonium bromide (CTAB) as a pore template and tetraethylortho silicate (TEOS) as a silica precursor. To evenly functionalize the interiors of the mesopores and place the hydrophobic PP inside the particles, the PP derivative was first coupled to the linker molecule aminopropyltriethoxysilane (APS), and then the coupled PP-APS molecules were added to the sol solution of the CTAB surfactant with TEOS during synthesis and allowed to co-condense into the silica framework.

In the resulting MSNs after surfactant removal, porphyrin molecules were attached to the inner walls of the two-dimensional hexagonal mesopores (Figure 5.2A). The spherical shapes

and sizes of the particles (50 - 100 nm in diameter) were imaged by transmission electron microscopy (TEM) (Figure 5.2B). The X-ray diffraction pattern exhibited a strong Bragg peak indexed as {100} at $2\theta = 2.1°$, corresponding to a d-spacing of ~ 4.2 nm. Existence of PP derivatives in the particles were confirmed by UV-Vis spectroscopy. It was calculated from the absorption peak of PP at ~ 403 nm that the particles contain ~ 0.5 wt % of the porphyrin derivatives (Figure 5.3).

5.3.2. Generation of Singlet Oxygen from the Photoexcited Porphyrin

The synthesized particles were then tested for the ability to generate singlet oxygen under photocontrol in solution, prior to cell studies. Singlet oxygen generation was first monitored by its luminescence emission spectra. To do that, PP-functionalized MSNs were dissolved in methanol or distilled water and placed in a cuvette, after which 10 mW, 514 nm light was directed to illuminate the particle suspension using an Argon laser. Luminescence emission of singlet oxygen was detected by the CCD detector. As shown in the Figure 5.4, the characteristic luminescence emission peak of singlet oxygen was observed in the infrared region (~ 1260 nm in methanol and ~ 1240 nm in water), which is in agreement with the reported spectra.[34] No peak was observed for underivatized particles.

Existence of singlet oxygen was also demonstrated by using a singlet oxygen trapping agent, 1,3-diphenylisobenzofuran (DPBF). Its reactivity to singlet oxygen and formation of endoperoxide has been well studied.[10,36] To set up a reaction, a suspension of the PP-derivatized MSN in methanol was mixed with DPBF (100 μM) and left in the dark or illuminated with ~ 5 mW/cm^2, 514 nm light for 30 min. After centrifugation of the particle suspension, the

supernatant solution containing DPBF was taken for the UV-Vis absorption measurement. As shown in the Figure 5.5, an absorption peak of DPBF at ~ 410 nm decayed after the particles were exposed to 514 nm light for 30 min, indicating that singlet oxygen was generated from the photoexcited PP and led to the oxidation of DPBF. Longer light illumination times led to greater oxidation of DPBF and larger decay of the absorption peak as shown in the Figure 5.6A. In addition, from plotting logarithmic DPBF concentration vs. illumination time (Figure 5.6B), a rate constant of the DPBF oxidation was calculated ($k = \sim 0.5 \times 10^{-5}/s$) with assumption of the first order kinetics. These results verify the capability of PP photosensitizer to produce singlet oxygen when it is attached to the pore walls of MSN.

5.3.3. Singlet Oxygen-induced Cell Death

After generation of singlet oxygen was confirmed in solution, *in vitro* cell studies were carried out in human pancreatic cancer cells (PANC-1). In an attempt to optimize the particle concentration to produce a sufficient quantity of singlet oxygen to induce cell death, PANC-1 cells were first incubated with two different concentrations (20 or 100 μg/ mL) of the PP-functionalized or unfunctionalized particles, and exposed to ~ 20 mW/cm^2, 647 nm red light using a Krypton laser for 0, 3, 5 or 10 min. For both concentrations, it was observed that no cells were damaged from the unfunctionalized particles. For the functionalized particles, when the particle concentration was low (i.e. 20 μg/ mL), a little to no cell death occurred except for 10 min light irradiation, indicating that the amount of generated singlet oxygen was negligible. At 100 μg/ mL of the concentration, ~ 40 % of cell death was observed from 3 min light illumination and rapidly increased to ~ 80 % from 10 min. Despite the dosage dependency, the

cell survival assay in the Figure 5.7 demonstrates successful generation of singlet oxygen by the PP inside of the cells, leading to cell death by the PDT mechanism.

5.3.4. Synergetic Cell Death by Singlet Oxygen and Anticancer Drug

In an effort to maximize cancer cell treatment utilizing the MSN-based PDT system, a second cancer therapy was incorporated into the PP-functionalized MSN utilizing the mesopore, which was loaded with CPT. It was reported that because of the hydrophobicity, CPT molecules that are loaded in the pores of MSN remain in the particles in aqueous cell culture media during incubation until they are taken up by cells.[37] Also in an earlier report in the Zink laboratory, ~ 0.06 wt % of CPT could be stored in the MSN that has a similar particle morphology prepared by the same synthetic condition except for the PP derivatization.[33] Based on the dosage-dependent cell test in the previous section, cells were incubated with a higher concentration, 100 μg/ mL, of the PP-functionalized particles loaded with CPT, and irradiated by ~ 20 mW/cm^2, 647 nm light for 0, 3, 5 or 10 min. The resulting cell survival was plotted as a function of the illumination time as shown in the Figure 5.8, and compared to that for the CPT-unloaded particles from Figure 5.5. In short, release of CPT from the particles increased cell death to a larger degree. Especially for 3 and 5 min, CPT release drastically increased cell death rate, almost doubling the amount of dead cells. About 70 % (or 80 %) of cell death was induced by the toxicities resulted from both CPT and singlet oxygen for the cells which were treated with 3 min (or 5 min) light illumination, while ~ 40 % (or ~ 50 %) from singlet oxygen only. After 10 min illumination, ~ 80 % of cells already died of singlet oxygen only, but with CPT release the cell death rised up to ~ 90 %. All of these results clearly show that CPT was released from the PP-derivatized pores in the cells and

induced apoptosis, leading to a synergetic effect on *in vitro* cancer cell treatment in cooperation with singlet oxygen molecules.

5.4. Summary

A bifunctional cancer treatment system of the photodynamics and chemotherapeutics can be assembled in the mesopores of a single silica nanoparticle and operated under photocontrol. The mesopores of the MSN were functionalized to include two types of the therapeutic agents, PP through a chemical bondage to the inner pore walls and CPT through a physical loading into the pores. Singlet oxygen generation of the PP-functionalized particles was confirmed by its luminescence emission spectra and the oxidation of the singlet oxygen probe molecule DPBF. When cancer cells were treated with the PP-functionalized particles loaded with CPT, both singlet oxygen and CPT simultaneously induced cell death, reducing the cell viability to a large degree in comparion to the particles with no CPT in the pores. The quantity of generated singlet oxygen relies on the concentration of the PP-derivatized particles and the light illumination time. The delivery and release capability of MSN in association with the PDT system offers a new strategy for constructing nanotherapeutic systems with a higher efficiencey in cancer treatment.

5.5. Experimental

5.5.1. Synthesis of the PP-functionalized MSN

0.1 g Protoporphyrin was first reacted with 20.5 mg N-hydrosuccinimide (NHS) and 34 mg ethyl(dimethylaminopropyl) carbodiimide (EDC) in 3 mL of dimethylsulfoxide (DMSO) at room temperature. To this mixture, 42 μL of APS was added and stirred 2 h at room temperature

under nitrogen in the dark. During this reaction, a surfactant solution was prepared in the other flask. 0.5 g of cetyltrimethylammonium bromide (CTAB), 1.75 mL of 2M NaOH, and 240 g of distilled water were mixed and stirred for 30 min at 80 °C. To this solution, 2.5 mL of triethylortho silicate (TEOS) and the coupled PP-APS were slowly added with vigorous stirring, followed by the addition of 0.63 mL of 3-trihydroxysilylpropyl methylphosphonate in 15 min. After 2 h reaction at 80 °C, the particles were filtered, thoroughly washed with deionized H_2O, and dried at 60 °C in the air. Template removal was accomplished by suspending 80 mg of the as-synthesized particles in 80 mL of MeOH with 0.8 mL of concentrated HCl and heating at 60 °C overnight. The surfactant-free particles were recovered by filtration, washing, and drying in the air.

5.5.2. Characterization of the synthesized PP-functionalized MSN

Powder X-ray diffraction measurements were carried out using a Panalytical X'Pert Pro powder diffractometer equipped with copper radiation ($K\alpha_1$ and $K\alpha_2$ = 1.5418 Å). Transmission electron microscope (TEM) image was collected on a JEM1200-EX (JEOL) instrument in the California NanoSystem Institute (CNSI). UV-Vis absorption spectra were collected using a Cary 5000 UV-Vis-NIR spectrophotometer. Luminescence emission spectra of singlet oxygen were obtained by using an Acton SpectraPro 2300i CCD and a coherent Argon Argon Innova 90C-5-excitation laser.

5.5.3. UV-Vis absorbance measurement of the photo-oxidation of DPBF

To measure the photo-oxidation of DPBF, a suspension of 1.5 mg of PP-derivatized MSN in 3 mL of methanol was mixed with DPBF (100 μM), and left in the absence of light

illumination or exposed to ~ 5mW, 514 nm light for 30 min. After centrifugation of the particle suspension, the supernatant solution containing DPBF was taken for the UV-Vis absorption measurement. A maximum absorption peak of DPBF was observed at ~ 410 nm.

5.5.4. In vitro toxicity assay

Human pancreatic cancer cells (PANC-1) were obtained from the American-type culture collection and were maintained in Dulbec- co's modified Eagle's medium (DMEM) (GIBCO) and Leibovitz's L-15 medium (Cellgro), respectively, supplemented with 10 % fetal calf serum (Sigma, MO), 2 % L-glutamine, 1 % penicillin, and 1 % streptomycin stock solutions with regular passage. 4000 cells were seeded in Lab-Tek chamber slide system for overnight before treated with 20 or 100 μg/ml PP-functionalized MSN that were unloaded or loaded with CPT. The CPT loading was processed by following our previously reported procedure.[22] The PANC-1 cells containing the particles were then irradiated by ~ 20 mW/cm^2, 647 nm light using a coherent Krypton Innova 300C laser for 0, 3, 5, or 10 min, and examined for cell viability by using the cell counting kit.[22]

5.6. Figures

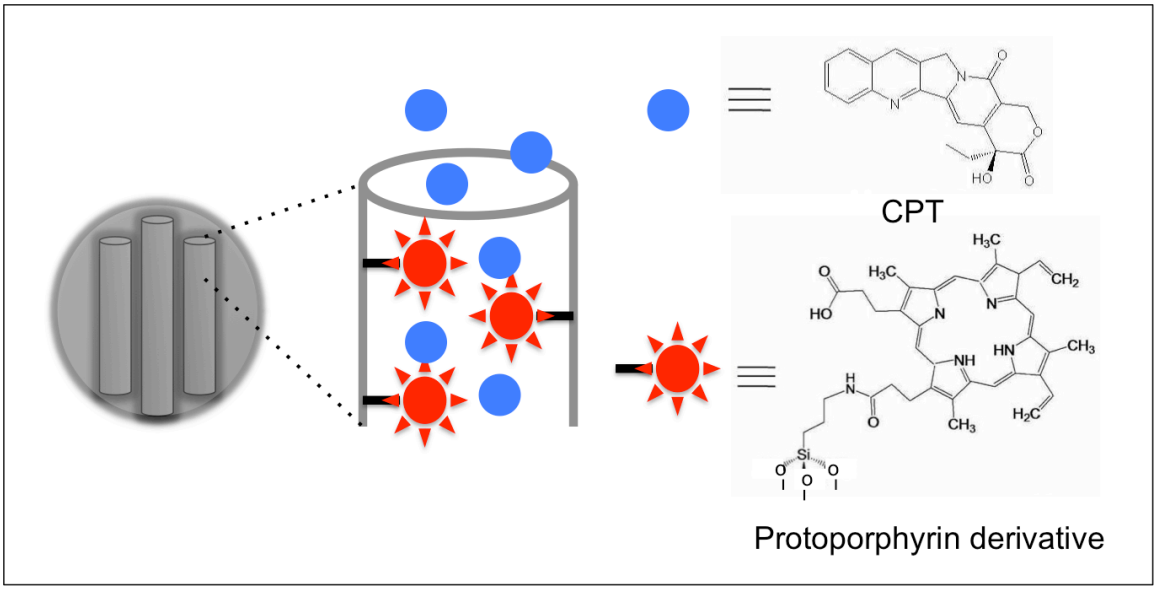

Figure 5.1. Pore interiors of the bifunctional MSN derivatized with a photosensitizer PP and loaded with an anticancer drug CPT. Light illumination at 647 nm stimulates PP to generate singlet oxygen that is harmful to cells. When CPT is released out of the pores inside of cells, cell apoptosis is induced maximizing a cell death rate in cooperation with the photoexcited PP derivative.

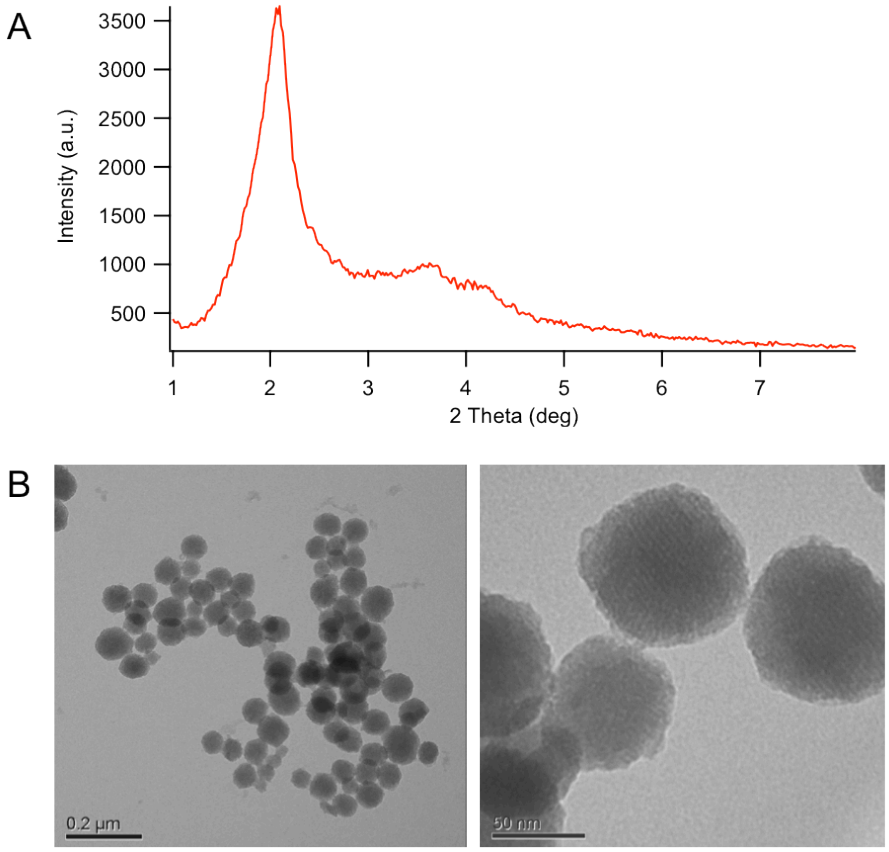

Figure 5.2. X-ray diffraction (XRD) pattern (A) and transmission electron microscopy (TEM) image (B) of the synthesized PP-derivatized MSN. From the XRD peaks, well-ordered structure of the mesopores was characterized with a strong Bragg peak indexed as {100} at $2\theta = 2.1°$. The spherical shapes and sizes of the particles (50 - 100 nm in diameter) were visualized by TEM.

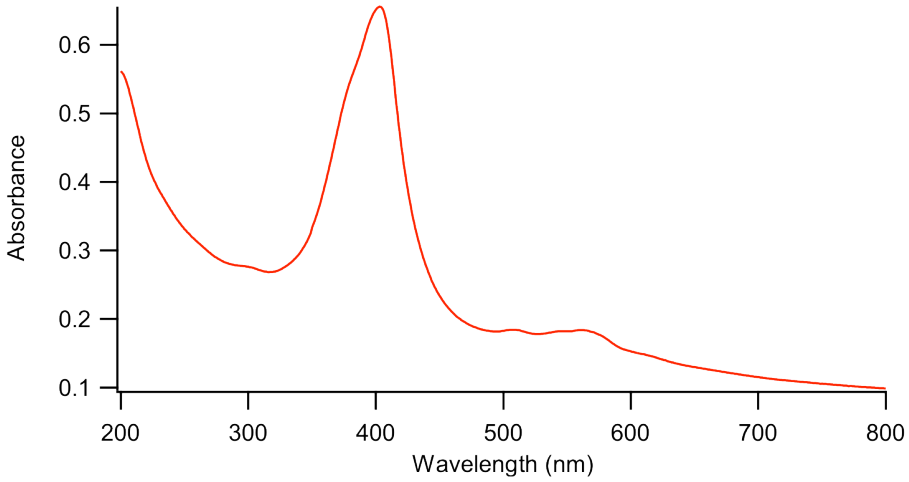

Figure 5.3. UV-Vis absorption spectrum of the PP-functionalized MSN. From the absorption maximum at ~ 403 nm, it was calculated that ~ 0.5 wt% of the PP derivatives were incorporated into the MSN.

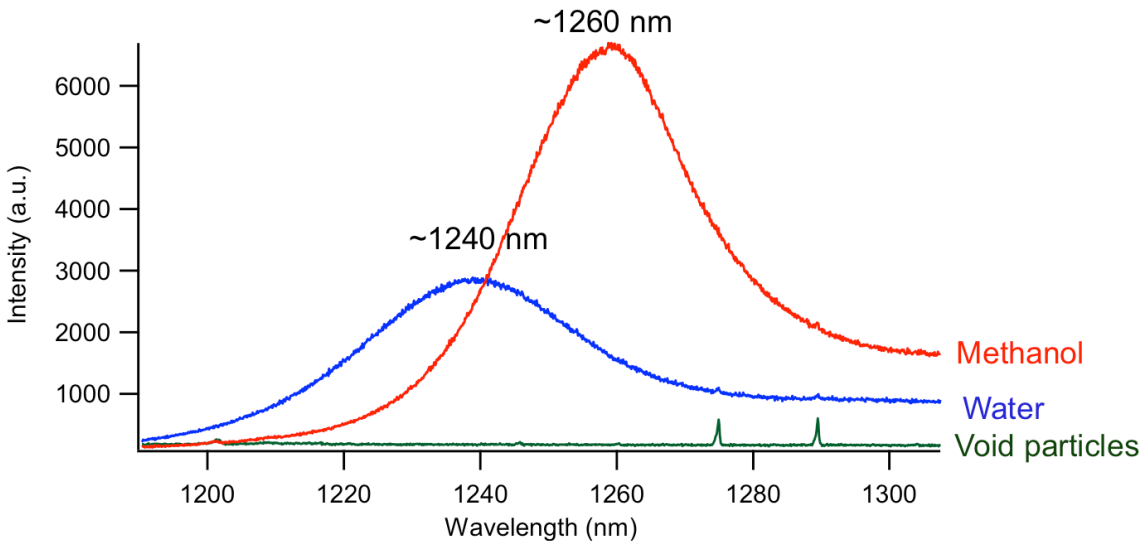

Figure 5.4. Infrared luminescence emission spectra of singlet oxygen generated from the photoexcited PP. The luminescence peak of singlet oxygen was observed from a suspension of the PP-functionalized MSN in methanol or distilled water when it was placed in a cuvette and illuminated by 514 nm light. When the underivatized MSN was tested in the same condition, no singlet oxygen peak was observed.

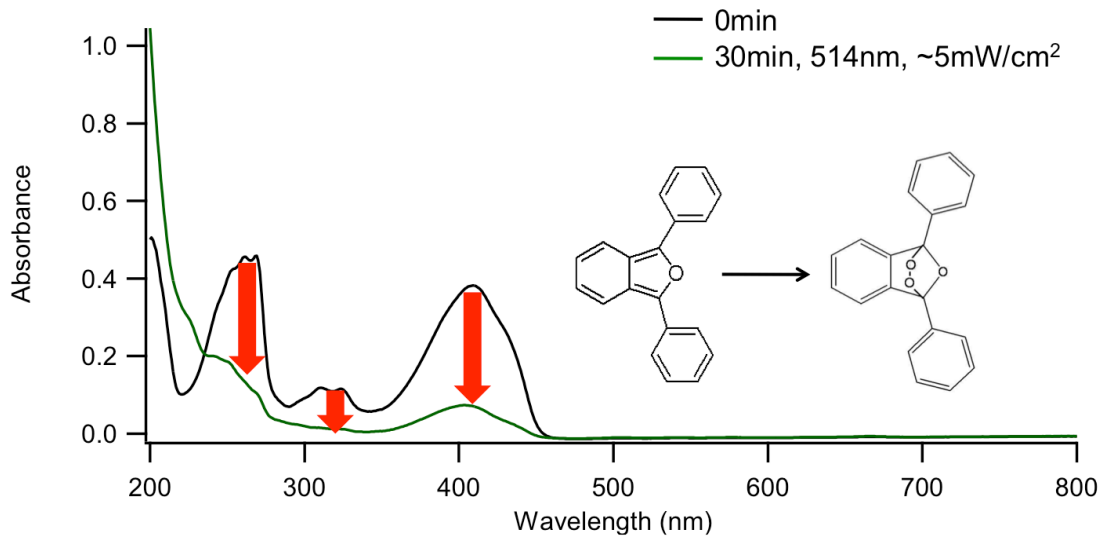

Figure 5.5. Photo-cycloaddtion of singlet oxygen to DPBF. A suspension of the PP-derivatized MSN in methanol was mixed with DPBF, and illuminated by 514 nm light for 30 min. After centrifugation of the particle suspension, the supernatant solution containing DPBF was taken for the UV-Vis absorption measurement. Decayed absorption peaks of the DPBF indicate that singlet oxygen was generated from the photoexcited PP, resulting in the oxidation of DPBF.

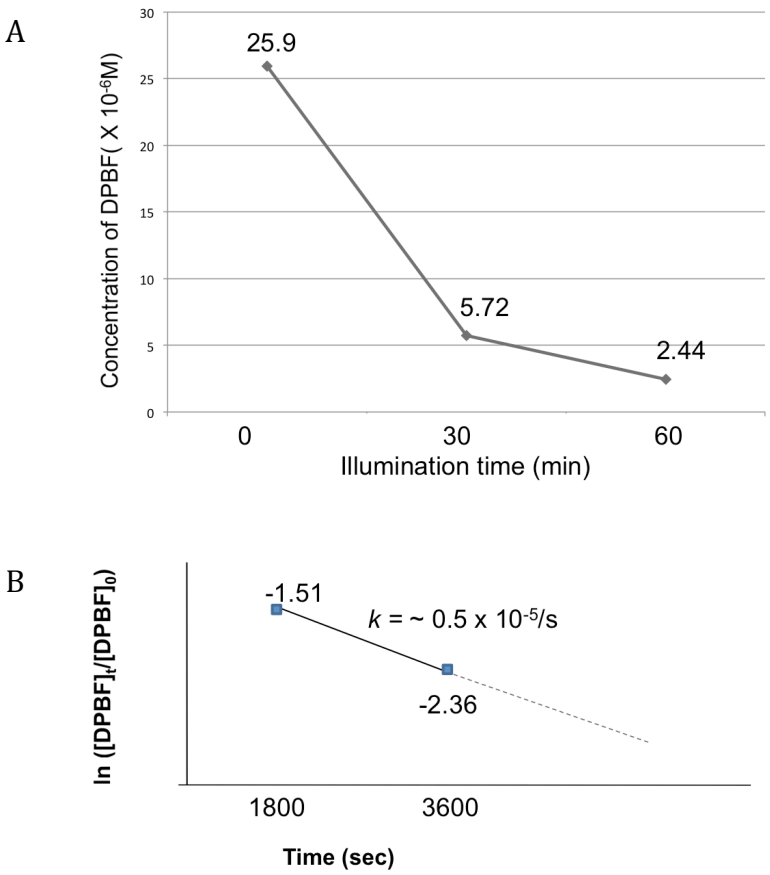

Figure 5.6. Decay profile of the photo-oxidized DPBF by singlet oxygen (A), and plotting of the first-order kinetics of the DPBF photo-oxidation (B). With increase of the light illumination time, greater decay of the DPBF absorption peak was obtained, indicating the decrease in the concentration of the unoxidized DPBF (A). From plotting of the logarithmic DPBF concentration vs. illumination, the calculated first-order rate constant *k* of the DPBF photo-oxidation by singlet oxygen was ~ 0.5 x 10^{-5} /s.

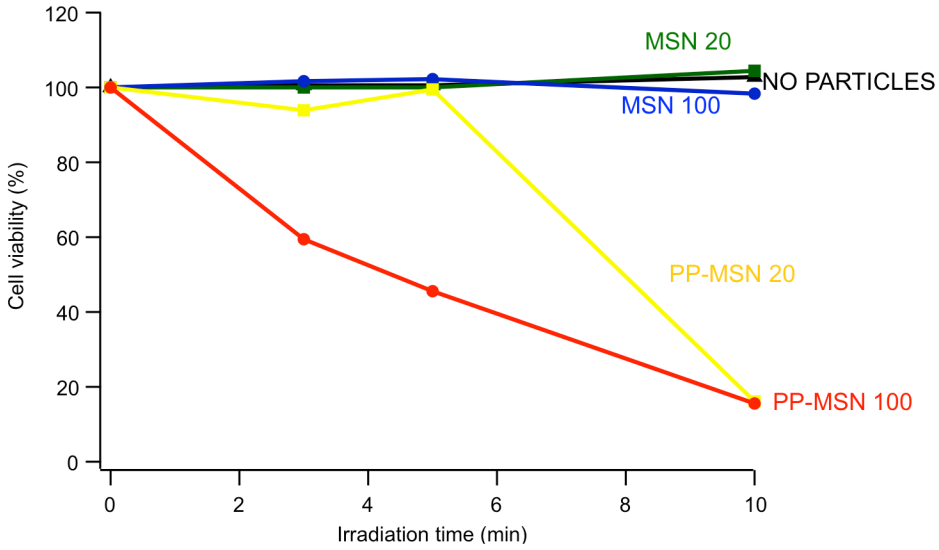

Figure 5.7. *In vitro* cytotoxicity assay of the PP-derivatized or underivatized MSNs. PANC-1 cancer cells were incubated with different concentrations (20 or 100 μg/ mL) of the PP-functionalized or unfunctionalized particles, and exposed to 647 nm light for 0, 3, 5 or 10 min. No cells were damaged from the unfunctionalized particles, but cell death was caused by the singlet oxygen molecules generated from the light-activated PP. When the particle concentration was low (i.e. 20 μg/ mL), a long illumination time (10 min) was required to generate the sufficient amount of singlet oxygen to cause cell death. When the concentration was high (100 μg/ mL), cell death occurred from a short illumination time (3 min) and the amount of dead cells increased with elongation of the illumination time. The cell viability was determined by using the cell counting kit.

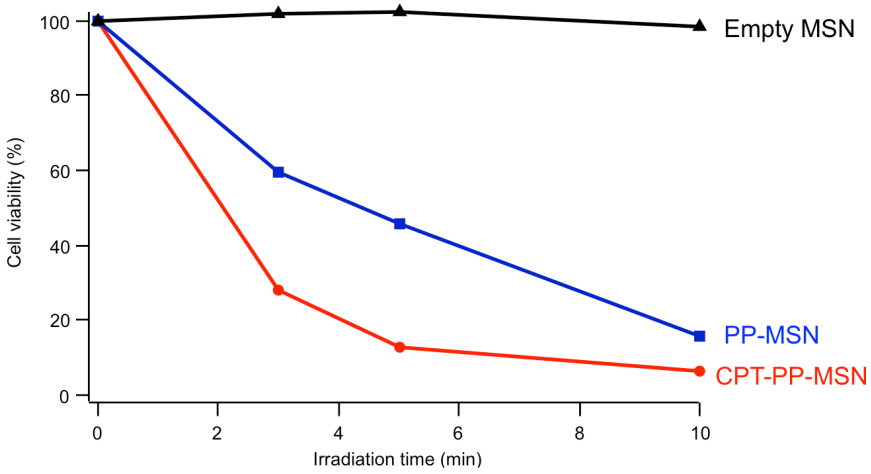

Figure 5.8. Cell survival from the PP-derivatized MSNs loaded with CPT. Cells were incubated with 100 μg/ mL) of the PP-functionalized particles loaded or unloaded with CPT, and illuminated with 647 nm light for 0, 3, 5 or 10 min. The red line for the CPT-unloaded particles was taken from the Figure 5.5 for comparison to the result from the CPT-loaded particles. The result indicates that both CPT and singlet oxygen function to induce cell death, leading to a synergetic cancer cell treatment. The cell viability was determined by using the cell counting kit.

5.7. References

[1] F. M. Muggia, I. Dimery, S. G. Arbuck, *Ann. N. Y. Acad. Sci.* **1996**, *803*, 213.

[2] N. Masuda, M. Fukuoka, Y. Kusunoki, K. Matsui, N. Takifuji, S. Kudoh, S. Negoro, M. Nishioka, K. Nakagawa, M. Takada, *J. Clin. Oncol.* **1992**, *10*, 1225–9.

[3] D. Abigerges, G. G. Chabot, J. P. Armand, P. Hérait, A. Gouyette, D. Gandia, *J. Clin. Oncol.* **1995**, *13*, 210–21.

[4] T. E. Keane, R. E. S. El-galley, C. Sun, J. A. Petros, D. Dillahey, A. Gomaa, S. A. M. D. G. Jr, W. P. M. I, *J. Urol.* **1998**, *160*, 252.

[5] K. D. Miller, S. E. Soule, L. G. Haney, P. Guiney, D. J. Murry, L. Lenaz, S.-L. Sun, G. W. Sledge Jr, *Invest. New Drugs* **2004**, *22*, 69–73.

[6] R. P. Hertzberg, M. J. Caranfa, K. G. Holden, D. R. Jakas, G. Gallagher, M. R. Mattern, S. Mong, J. O. L. Bartus, R. K. Johnson, W. D. Kingsbury, *J. Med. Chem.* **1989**, *32*, 715–720.

[7] N. Liu, D. R. Dunphy, P. Atanassov, S. D. Bunge, Z. Chen, G. P. Lo, T. J. Boyle, C. J. Brinker, *Nano Lett.* **2004**, *4*, 551–554.

[8] A. Guiotto, M. Canevari, P. Orsolini, O. Lavanchy, C. Deuschel, N. Kaneda, A. Kurita, T. Matsuzaki, T. Yaegashi, S. Sawada, et al., *J. Med. Chem.* **2004**, *47*, 1280–9.

[9] S. Wang, R. Gao, F. Zhou, M. Selke, *J. Mater. Chem.* **2004**, *14*, 487.

[10] W. Spiller, H. Kliesch, D. Wohrele, S. Hackbarth, B. Roder, G. J. Schnurpfeil, *J. Porphyrins Phtahlocyanines* **1998**, *2*, 145–158.

[11] K. Wang, Q. He, X. Yan, Y. Cui, W. Qi, L. Duan, J. Li, *J. Mater. Chem.* **2007**, *17*, 4018.

[12] A. Derycke, *Adv. Drug Deliv. Rev.* **2004**, *56*, 17–30.

[13] Y. Choi, J. R. McCarthy, R. Weissleder, C.-H. Tung, *ChemMedChem* **2006**, *1*, 458–63.

[14] C. Vannostrum, *Adv. Drug Deliv. Rev.* **2004**, *56*, 9–16.

[15] J. Taillefer, M. C. Jones, N. Brasseur, J. E. van Lier, J. C. Leroux, *J. Pharm. Sci.* **2000**, *89*, 52–62.

[16] T. Y. Ohulchanskyy, I. Roy, L. N. Goswami, Y. Chen, E. J. Bergey, R. K. Pandey, A. R. Oseroff, P. N. Prasad, *Nano Lett.* **2007**, *7*, 2835–42.

[17] I. Roy, T. Y. Ohulchanskyy, H. E. Pudavar, E. J. Bergey, A. R. Oseroff, J. Morgan, T. J. Dougherty, P. N. Prasad, *J. Am. Chem. Soc.* **2003**, *125*, 7860–5.

[18] Y. N. Konan, R. Gurny, E. Allémann, *J. Photochem. Photobiol. B.* **2002**, *66*, 89–106.

[19] M. H. Huang, B. S. Dunn, H. Soyez, J. I. Zink, **1998**, 7331–7333.

[20] J. S. B. C.T. Kresge, M.E. Leonowicz, W.J. Roth, J.C. Vartuli, *Nature* **1992**, *359*, 710–712.

[21] Y. Lu, R. Ganguli, C. Drewien, M. Anderson, J. I. Zink, *Nature* **1997**, *389*, 651–655.

[22] J. Lu, E. Choi, F. Tamanoi, J. I. Zink, *Small* **2008**, *4*, 421–426.

[23] E. Choi, J. Lu, F. Tamanoi, J. I. Zink, *Zeitschrift für Anorg. und Allg. Chemie* **2014**, n/a–n/a.

[24] D. Tarn, M. Xue, J. I. Zink, *Inorg. Chem.* **2013**, *52*, 2044–9.

[25] L. Mu, S. S. Feng, *J. Control. Release* **2003**, *86*, 33–48.

[26] S. Febvay, D. M. Marini, A. M. Belcher, D. E. Clapham, *Nano Lett.* **2010**, *10*, 2211–9.

[27] C. R. Thomas, D. P. Ferris, J.-H. Lee, E. Choi, M. H. Cho, E. S. Kim, J. F. Stoddart, J.-S. Shin, J. Cheon, J. I. Zink, *J. Am. Chem. Soc.* **2010**, *132*, 10623–5.

[28] J. Kim, H. S. Kim, N. Lee, T. Kim, H. Kim, T. Yu, I. C. Song, W. K. Moon, T. Hyeon, *Angew. Chem. Int. Ed. Engl.* **2008**, *47*, 8438–41.

[29] M. Liong, S. Angelos, E. Choi, K. Patel, J. F. Stoddart, J. I. Zink, *J. Mater. Chem.* **2009**, *19*, 6251.

[30] M. Liong, B. France, K. a. Bradley, J. I. Zink, *Adv. Mater.* **2009**, *21*, 1684–1689.

[31] Z. Li, J. N. Likoko, A. a Hwang, D. P. Ferris, S. Yang, G. Derrien, C. Charnay, J.-O. Durand, J. I. Zink, *J. Phys. Chem. C. Nanomater. Interfaces* **2011**, *115*, 19496–19506.

[32] H. Meng, M. Xue, T. Xia, Z. Ji, D. Y. Tarn, J. I. Zink, A. E. Nel, *ACS Nano* **2011**, *5*, 4131–44.

[33] J. Lu, M. Liong, J. I. Zink, F. Tamanoi, *Small* **2007**, *3*, 1341–6.

[34] H.-L. Tu, Y.-S. Lin, H.-Y. Lin, Y. Hung, L.-W. Lo, Y.-F. Chen, C.-Y. Mou, *Adv. Mater.* **2009**, *21*, 172–177.

[35] S. Angelos, E. Choi, F. Vo, L. De Cola, J. I. Zink, *J. Phys. Chem. C* **2007**, *111*, 6589–6592.

[36] D. B. Tada, L. L. R. Vono, E. L. Duarte, R. Itri, P. K. Kiyohara, M. S. Baptista, L. M. Rossi, *Langmuir* **2007**, *23*, 8194–9.

[37] M. Liong, J. Lu, M. Kovochich, T. Xia, S. G. Ruehm, A. E. Nel, F. Tamanoi, J. I. Zink, *ACS Nano* **2008**, *2*, 889–96.